
CT Technology for Imaging the Thorax: State of the Art

Thomas G. Flohr and Bernhard Schmidt

Abstract

We review the basics of CT system design, scan, and image reconstruction techniques, as well as scan protocols for imaging of the thorax with multi-detector row CT (MDCT) systems. In addition, we discuss CT systems with wide area detectors and dual-source CT (DSCT). We briefly describe different techniques to reduce the radiation dose in thoracic CT, and we discuss dual energy CT acquisition techniques which have the potential to provide combined functional and morphological information, e.g., to depict local perfusion deficits in the lung parenchyma in patients with pulmonary embolism.

1 Introduction

The advent of spiral computed tomography (CT) in 1990 and the broad introduction of multi-detector row computed tomography (MDCT) in 1998 were significant steps in the ongoing refinement of CT-imaging techniques of the thorax.

With the first generation of 4-slice CT systems, high-resolution imaging of the entire thorax within one breath-hold of the patient became feasible, and CT was quickly recognized as the gold standard for the diagnosis of pulmonary embolism up to the level of sub-segmental arteries (Schoepf et al. 2002; Remy-Jardin et al. 2002).

ECG-synchronized data acquisition (Ohnesorge et al. 2000), which proved to be sufficient for adequate visualization of the coronary arteries at low to moderate heart rates (Achenbach et al. 2000; Becker et al. 2000; Knez et al. 2001; Nieman et al. 2001), could unfortunately not be extended to the entire thorax because of slow scan speed.

The generation of 16-slice MDCT systems (Flohr et al. 2002a, b) provided simultaneous acquisition of 16 submillimeter slices and faster gantry rotation with rotation times down to 0.375 s. CT scans of the entire thorax with submillimeter spatial resolution were now possible in about 10 s. As a consequence, central and peripheral pulmonary embolism could be reliably and accurately diagnosed even in dyspneic patients with limited ability to cooperate (Remy-Jardin et al. 2002; Schoepf et al. 2003). The combined assessment of pulmonary embolism and deep venous thrombosis, first demonstrated in 2001 (Schoepf et al. 2001), entered clinical routine. The faster scan speed of ECG-gated cardiac scanning with 16 slices enabled motion-free visualiza-

T.G. Flohr (✉)
Siemens Healthcare GmbH, Computed Tomography,
CT Concepts Department, Forchheim, Germany

Department of Interventional Radiology,
Eberhard-Karls-University, Tübingen, Germany
e-mail: thomas.flohr@siemens.com

B. Schmidt
Siemens Healthcare GmbH, Computed Tomography,
CT Concepts Department, Forchheim, Germany

tion of the lung and the cardiothoracic vessels as well as cardiac functional evaluation in one scan, even though detailed visualization of the coronary arteries was still limited (Coche et al. 2005).

Sixty-four-slice CT systems, available since 2004, enabled CT imaging of the thorax with isotropic submillimeter spatial resolution in less than 5 s scan time. This facilitated the examination of uncooperative patients and emergency patients, e.g., with suspicion of acute pulmonary embolism. The improved temporal resolution due to gantry rotation times down to 0.33 s increased the clinical robustness of ECG-gated scanning at higher heart rates, even though most authors still proposed the administration of beta-blockers (Leber et al. 2005; Raff et al. 2005). Sixty-four-slice CT scanners enabled comprehensive diagnosis of morphology and cardiac function within one integrated CT examination, including high-resolution imaging of the coronary arteries (Salem et al. 2006; Bruzzi et al. 2006a, b; Delhaye et al. 2007). ECG-gated 64-slice CT was also used for rapid triage of patients with acute chest pain in the emergency room and for diagnosis of pulmonary embolism, aortic dissection or aneurysm, or significant coronary artery disease in one scan. This application is often referred to as “triple rule out” (Schoepf 2007; Johnson et al. 2007a). As a downside, ECG-gated MDCT scanning of the entire thorax can result in considerable radiation exposure, which is of particular concern in patients with low likelihood of disease.

Even with 64-slice CT, motion artifacts remained an important challenge for cardiothoracic imaging. In 2005, a dual-source CT (DSCT) system, i.e., a CT system with two x-ray tubes and two corresponding detectors offset by 90°, was introduced (Flohr et al. 2006). It provided improved temporal resolution of 83 ms independent of the patient’s heart rate as compared to 165–190 ms with MDCT systems at that time. DSCT scanners proved to be well suited for integrated cardiothoracic examinations even in acutely ill patients and for the triage of patients with acute chest pain (Johnson et al. 2007b). The introduction of dual-energy scanning with DSCT enabled tissue characterization and provided combined functional and morphological information, e.g., to depict local perfusion deficits in the lung parenchyma in patients with pulmonary embolism (Pontana et al. 2008; Thieme et al. 2008).

The second and third generations (introduced in 2009 and 2013, respectively) of DSCT systems offer high-pitch scan modes which enable high-resolution CT scans of the entire thorax in less than 1 s scan time with an acquisition time per image better than 100 ms (Lell et al. 2009; Tacelli et al. 2010). These scan modes are potentially advantageous for evaluating the lung parenchyma and vascular structures in patients who have difficulty complying with breath-holding instructions (Schulz et al. 2012). High-pitch scan modes have been used for fast CTA scans of the aorta (Beeres et al. 2012). Combined with ECG triggering, they provide adequate visualization of the coronary arteries, the aorta, and the iliac arteries in one scan at low radiation dose, which is beneficial in the planning of transcatheter aortic valve replacement (TAVR) procedures (Wuest et al. 2012; Plank et al. 2012).

Since 2009, iterative reconstruction techniques have been used to significantly reduce the radiation dose in CT examinations of the thorax (e.g., Prakash et al. 2010; Leipsic et al. 2010; Pontana et al. 2011a, b, 2015; Singh et al. 2011; Baumueller et al. 2012). With the latest generation of iterative reconstruction and dedicated pre-filtration of the x-ray beam, radiation dose values of 0.1 mSv and less have been reported for non-enhanced CT scans of the thorax (Newell et al. 2015).

Yet another challenge for CT is the visualization of dynamic processes in extended anatomical ranges, e.g., to characterize the inflow and outflow of contrast agent in the arterial and venous systems in dynamic CT angiographies or to determine the enhancement characteristics of the contrast agent in volume perfusion studies. One way to address this problem is the introduction of area detectors large enough to cover organs such as the heart, the kidneys, or the brain in one axial scan. Meanwhile, two vendors have introduced CT scanners with 16 cm detector coverage at isocenter, providing 320×0.5 mm collimation at 0.27 s rotation time or 256×0.625 mm collimation at 0.28 s rotation time. These scanners have the potential to acquire dynamic volume data by repeatedly scanning the same anatomical range without table movement (e.g., Ohno et al. 2011; Willems et al. 2012; Motosugi et al. 2012). An alternative to provide time-resolved CT data of larger anatomical volumes is a periodic shuttle movement of the patient table while scan data are acquired (e.g., Goetti

et al. 2012; Morhard et al. 2010; Sommer et al. 2010, 2012). This technique is realized in several CT systems with smaller detector z -coverage.

Overall, the greatest challenge of evolving CT technology is the explosion of information now available to physicians. Standardizing the display of post-processed images will be increasingly important to preserve efficient workflow and optimum patient care.

2 CT System Technology

2.1 Multi-Detector Row CT (MDCT)

In this section, we review the basics of CT system design, scan, and image reconstruction techniques, as well as scan protocols for imaging of the thorax with multi-detector row CT (MDCT) systems. In our terminology, these are CT systems with 2–128 detector rows and a detector z -coverage of up to 8 cm at isocenter. CT systems with wider detectors (e.g., 320×0.5 mm or 256×0.625 mm, both covering 16 cm) and dual-source CT (DSCT) systems will be discussed in a separate section because of their different clinical protocols.

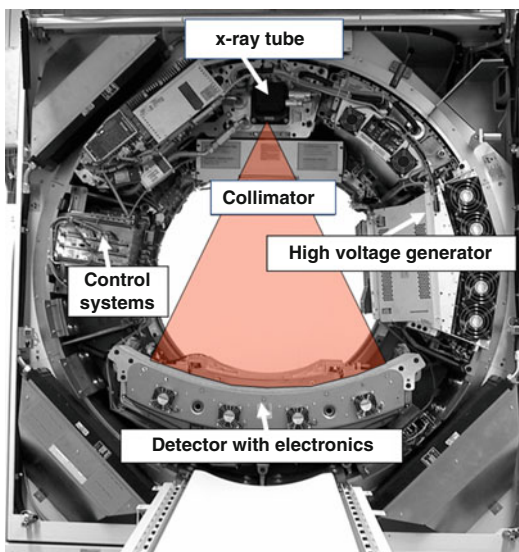


Fig. 1 Basic system components of a modern MDCT system. The x-ray fan beam is indicated in red; it covers a SFOV of typically 50 cm in diameter. The data measurement system consists of detector and detector electronics

2.1.1 MDCT System Design

The basic system components of a modern MDCT system are shown in Fig. 1. Today, the third-generation fan-beam CT design is used by all manufacturers, characterized by an x-ray tube and an opposing detector which are mounted on a rotating gantry ring. The detector is a two-dimensional array, consisting of 2–128 rows aligned in the z -axis direction (the z -axis is the patient's longitudinal axis) with 700 and more detector elements in each row. The fan angle of the detector is wide enough (approximately 45 – 55°) to cover a whole-body scan field of view (SFOV) of usually 50 cm in diameter. In a CT scan, the detector array measures the x-ray attenuation profile of the patient at about 1000–2000 different angular positions during a 360° rotation. All measurement values acquired at the same angular position of the measurement system are called a “projection” or “view.” Slip-ring designs which pass the electrical signals across sliding contacts allow for continuous rotation of the measurement system.

State-of-the art x-ray tubes are powered by onboard generators and provide peak powers of 60–120 kW at different user-selectable voltages ranging from 80 to 140 kV. Recently, the available voltage range was extended to enable new clinical applications, and other tube voltages such as 70 kV became available. Scanning at low tube voltage is favorable for dose-efficient pediatric CT (Niemann et al. 2014; Durand and Paul 2014). In addition, contrast-enhanced examinations can be performed at reduced radiation dose and potentially reduced amount of contrast agent, because the x-ray attenuation of iodine significantly increases at lower kV (Meyer et al. 2014). This technique will be described in detail in Sect. 3.1.

All modern MDCT systems use solid-state scintillation detectors. The x-rays hit a radiation-sensitive crystal or ceramic (such as gadolinium oxide, gadolinium oxysulfide, or garnets) with suitable doping. They are absorbed, and their energy is converted into visible light which is detected by a Si photodiode attached to the backside of the detector. The resulting electrical current is amplified and converted into a digital signal.

Key requirements for a detector material are good detection efficiency, i.e., high atomic number, and very short afterglow time to enable fast

readout at the high gantry rotation speeds that are essential for cardiothoracic CT.

The image noise in a CT image is caused by the quantum noise of the x-ray photons and the electronic noise of the detection system. In high-dose scanning situations, the image noise is dominated by quantum noise. Electronic noise significantly contributes to the image noise when bigger patients are scanned or in examinations at low radiation dose, e.g., in low-dose thorax scans. In addition, electronic noise degrades image quality and the stability of CT values. Recently, a detector with integrated electronics was commercially introduced (STELLAR, Siemens Healthcare, Forchheim, Germany), with the goal to reduce electronic noise and detector cross talk. In this design, photodiodes and analog-to-digital

converters are combined and directly attached to the ceramic scintillators, without the need of noise-sensitive analog connection cables (see Fig. 2). In a recent study, image noise reduction by up to 40% for a 30 cm phantom corresponding to an average abdomen was demonstrated with the use of a detector with integrated electronics at 80 kV (Duan et al. 2013). According to the authors, this noise reduction translated into up to 50% in dose reduction to achieve equivalent image noise.

A CT scanner must provide different slice widths to adapt scan speed and through-plane (z -axis) resolution to the clinical requirements of different scan protocols. In MDCT, detectors with a larger number of detector rows than finally read-out slices are used to provide slices

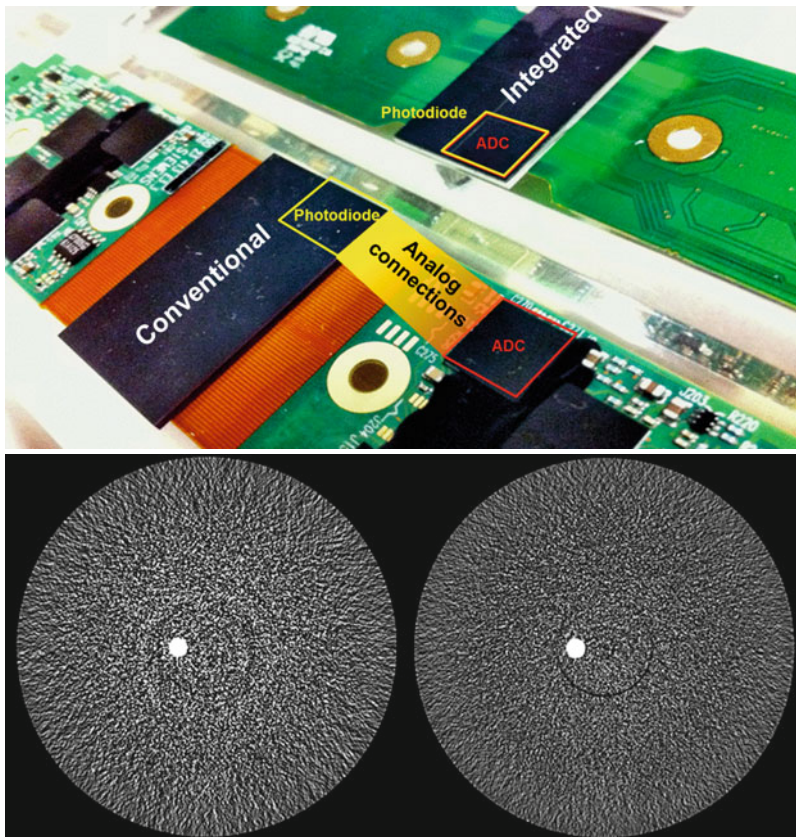


Fig. 2 *Top*: Principle of an integrated CT detector compared to a conventional CT detector. The Si tile is shown without the scintillation ceramics. Integrated detectors do not use distributed electronics with analog connections. As

a consequence, electronic noise and cross talk are reduced. *Bottom*: Image quality improvement in a 40 cm phantom with an integrated detector (*right*) as compared to a conventional detector (*left*). Scan parameters: 80 kV, 100 mAs

at different collimated slice widths. The total beam width in the z -direction is adjusted by pre-patient collimation, and the signals of every two (or more) detectors along the z -axis are electronically combined to thicker slices.

The detector of a 16-slice CT (Siemens SOMATOM Emotion 16) as an example comprises 16 central rows, each with 0.6 mm collimated slice width, and four outer rows on either side, each with 1.2 mm collimated slice width – in total, 24 rows with a z -width of 19.2 mm at isocenter (Fig. 3). By adjusting the x-ray beam width such that only the central detector rows are illuminated, the system provides 16 collimated 0.6 mm slices (Fig. 3, top). By illuminating the entire detector, reading out all rows, and electronically combining the signals of every two central rows, the system provides 16 collimated 1.2 mm slices (Fig. 3, bottom). The 16-slice detectors of other manufacturers are similarly designed, with slightly different collimated slice widths (0.5, 0.6, or 0.625 mm, depending on the manufacturer).

MDCT detectors with 64 detector rows provide 64 collimated 0.5, 0.6, or 0.625 mm slices. They allow acquisition of 32 collimated 1.0, 1.2,

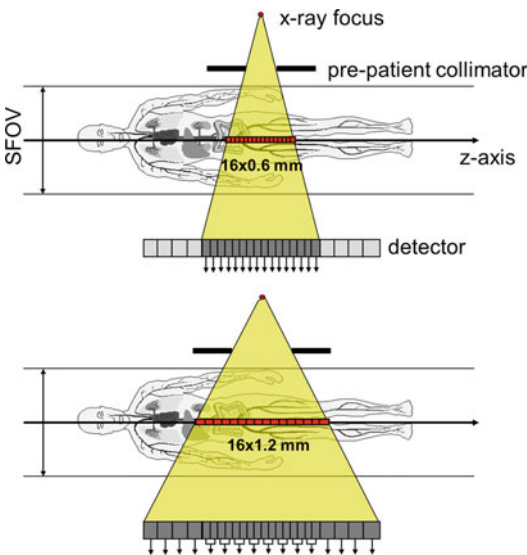


Fig. 3 Example of a 16-slice detector, which consists of 24 detector rows and provides either 16 collimated 0.6 mm slices (top) or – by combination of the signals of every two central rows – 16 collimated 1.2 mm slices (bottom)

or 1.25 mm slices by electronic combination of every two detector rows. One CT system has a detector with 128 collimated 0.625 mm slices (total z -width 8 cm at isocenter). The widest commercially available CT detectors cover 16 cm at isocenter; they acquire 320 collimated 0.5 mm slices (Aquilion ONE, Toshiba Medical, Japan) or 256 collimated 0.625 mm slices (Revolution, GE Healthcare, USA).

All modern MDCT scanners enable reconstruction of images with different slice widths from the same raw data – typically, the scan data are acquired at submillimeter collimation (e.g., 64×0.6 mm, or 64×0.625 mm), and different sets of image data are reconstructed with different target slice widths according to the clinical needs (e.g., 3 or 5 mm for initial viewing and additional submillimeter slices or 1 mm slices for post-processing).

Some CT systems double the number of simultaneously acquired slices by using special “conjugate” interpolation schemes during image reconstruction or by means of a z -flying focal spot (Flohr et al. 2004, 2005). The focal spot in the x-ray tube is periodically moved between two z -positions on the anode plate by electromagnetic deflection. As a consequence, the measurement rays of two readings are shifted by half a collimated slice width at isocenter and can be interleaved to one projection with double the number of slices, but half the z -sampling distance (Fig. 4). Two 64-slice readings with 0.6 mm slice width and 0.6 mm z -sampling distance, as an example, are combined to one projection with 128 overlapping 0.6 mm slices at 0.3 mm z -sampling distance.

The z -flying focal spot provides improved data sampling in the z -direction for better through-plane resolution and reduced spiral windmill artifacts (see Fig. 5).

2.1.2 MDCT Scan and Image Reconstruction Techniques

With the advent of MDCT, axial “step-and-shoot” scanning has remained in use for only few clinical applications, such as ECG-triggered cardiac scans at low radiation dose. For the vast majority of all MDCT examinations, spiral (helical) scanning is the method of choice.

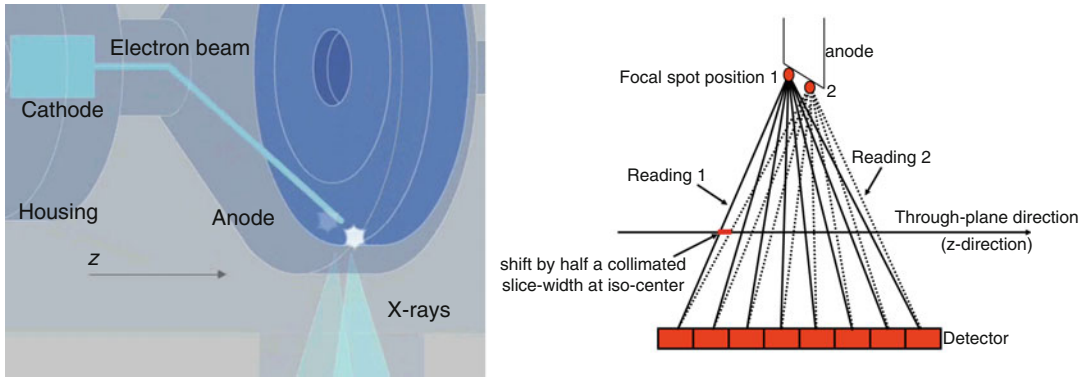


Fig. 4 Principle of a z -flying focal spot. Consecutive readings are shifted by half a collimated slice width (at isocenter) by means of a periodic motion of the focal spot

on the anode plate. Every two readings are interleaved to one projection with double the number of slices and half the z -sampling distance

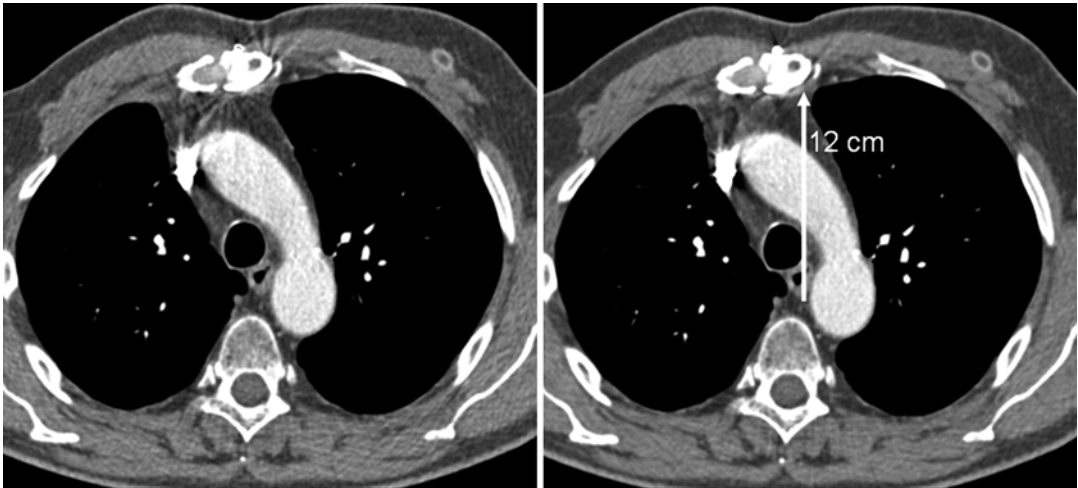


Fig. 5 Reduction of spiral windmill artifacts in a 64-slice CT scan (left) with the z -flying focal spot technique (right, white arrow). The distance of the sternum from the isocenter is about 12 cm

An important parameter to characterize a spiral scan is the pitch p . It is given by $p = \text{tablefeed per rotation} / \text{total } z\text{-width of the collimated beam at isocenter}$

This definition applies to single-slice CT as well as to MDCT. It indicates whether scan data are acquired with gaps ($p > 1$) or with overlap ($p < 1$) in the through-plane direction. If the x-ray tube current is left unchanged, radiation dose increases with decreasing pitch due to the overlapping radiation. Some CT scanners (e.g., Siemens MDCT systems) compensate for this increase by automatically lowering the tube cur-

rent with decreasing pitch such that a constant; pitch-independent “reference mAs” and radiation dose are applied.

Many technical challenges of MDCT image reconstruction, such as the complicated z -sampling patterns or the cone-angle problem, have been addressed in the past 15 years. In two-dimensional image reconstruction approaches used for single-slice CT, all measurement rays are perpendicular to the z -axis. In MDCT systems, however, the measurement rays are tilted by the so-called cone angle with respect to a plane perpendicular to the z -axis. The wider the

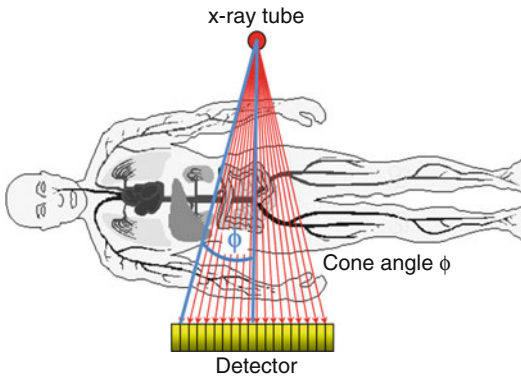


Fig. 6 Geometry of a MDCT scanner demonstrating the cone-angle problem: in the patient's longitudinal direction (z -direction), the measurement rays are tilted by the so-called cone-angle ϕ with respect to a plane perpendicular to the z -axis

detector is in the z -direction, i.e., the more detector rows it has, the larger is the cone angle of the outer detector rows (Fig. 6).

For CT systems with up to eight simultaneously acquired slices, cone-beam artifacts stay at a clinically acceptable level if the cone angle of the measurement rays is simply neglected in the image reconstruction algorithms. The rays are then treated as if they were perpendicular to the z -axis. For CT systems with more than eight slices, the cone angle has to be taken into account at least approximately. Pertinent reconstruction methods considering the cone-beam geometry are nutating slice algorithms (e.g., Flohr et al. 2003) and 3D-filtered back projection (Stierstorfer et al. 2004). Nowadays, 3D-filtered back projection is the reconstruction method of choice for most MDCT systems (Grass et al. 2000; Hein et al. 2003; Stierstorfer et al. 2004). 3D-filtered back projection is a natural extension of the 2D-filtered back projection used in single-slice CT reconstruction: the measurement rays are back projected into a 3D volume along the lines of measurement, in this way accounting for their cone-beam geometry. 3D-filtered back projection, even though it is an approximate algorithm, can significantly reduce cone-beam artifacts. In most MDCT scanners, 3D-filtered back projection is enhanced by z -filtering techniques which enable the reconstruction of images

with different slice widths from the same CT raw data. The user can then trade off z -axis resolution with image noise.

2.1.3 Scan Protocols for MDCT Imaging of the Thorax

CT imaging of the thorax benefits from MDCT technology in several ways:

- *Shorter scan time.* Examination times for standard protocols can be significantly reduced. With modern MDCT systems, the entire thorax can be scanned at submillimeter isotropic resolution in less than 5 s. CT angiographic examinations benefit from these short scan times, because a compact contrast bolus may be used.
- *Extended scan range.* Larger scan ranges can be examined within one breath-hold time of the patient. This is relevant for CT angiography with extended coverage and for oncological staging. The chest and abdomen, as an example, can be examined in one scan with one contrast bolus.
- *Improved through-plane resolution.* The most important clinical benefit is the ability to scan a region of interest, e.g., the chest, within a breath-hold time of the patient with substantially thinner slices than in single-slice CT. The significantly improved through-plane resolution is beneficial for all reconstructions, in particular when 3D post-processing is part of the clinical protocol.

In clinical practice, most scan protocols benefit from a combination of these advantages. The close-to or true isotropic spatial resolution in routine examinations – depending on the number of detector rows – enables 3D renderings of diagnostic quality and oblique multiplanar reformations (MPRs) with a resolution comparable to the axial images. The wide availability of MDCT systems has transformed CT from a modality acquiring cross-sectional slices of the patient to a volume imaging modality. In many scan protocols, the use of narrow collimation is recommended independently of what slice width is desired for primary viewing. In practice, different

slice widths are commonly reconstructed by default: thick slices for PACS archiving and primary viewing and thin slices for 3D post-processing and evaluation.

MDCT imaging of the thorax also greatly benefits from the shorter gantry rotation times of modern MDCT scanners and the reduced acquisition times per image. The better the temporal resolution of the images, the less pronounced are motion artifacts in CT images of the thorax, which typically appear as double contours or blurring of thoracic structures close to the heart. The best possible temporal resolution in a single-source CT scan is half the rotation time of the respective scanner, because half a rotation of scan data is the minimum needed for image reconstruction close to the isocenter. CT scanners used for thoracic imaging should therefore enable short gantry rotation times – at the moment, rotation times of 0.25–0.3 s result in a best possible temporal resolution of 125–150 ms. A further significant improvement of the temporal resolution to values below 100 ms can be achieved with dual-source CT systems (see Fig. 7) (Adapted from Hutt et al. 2016).

It is interesting to note that the temporal resolution in a spiral scan, which is the basic scan mode for MDCT scanning of the thorax, depends on the pitch of the scan: the higher the pitch, the better the temporal resolution. At a pitch of 1, a full rotation of scan data typically contributes to an image. Temporal resolution is therefore not better than the gantry rotation time. The higher the pitch, the less data contribute to image reconstruction, and the temporal resolution approaches half the gantry rotation time. On the other hand, even lower pitch will lead to even worse temporal resolution: at a pitch of 0.5, almost two rotations of scan data contribute to an image. Therefore, to reduce motion artifacts, it is mandatory to perform MDCT examinations of the thorax at fast gantry rotation and high pitch >1 . Another option, in particular when the heart and the coronary arteries are also targeted in the planned examination, is the use of ECG-gated scan protocols. As a downside, these protocols result in longer scan times and increased radiation dose to the patient. ECG-triggered high-pitch scan protocols are a potential way out of this dilemma – they will be discussed in Sect. 2.3.

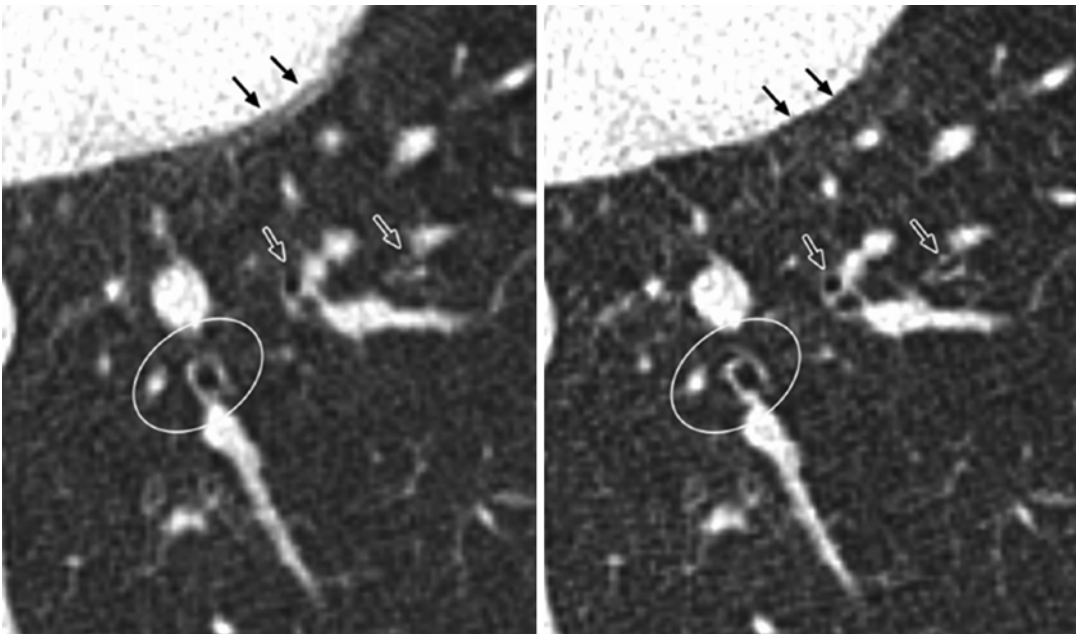


Fig. 7 Lung image acquired with a dual-source CT and reconstructed at a temporal resolution of 140 ms (*left*) and 75 ms (*right*). Note the double contour of the left ventricu-

lar wall due to cardiac motion (*fine arrows*) and the blurry appearance of the bronchi (*arrows*) in the image at 140 ms temporal resolution (Modified from (Hutt et al. 2016))

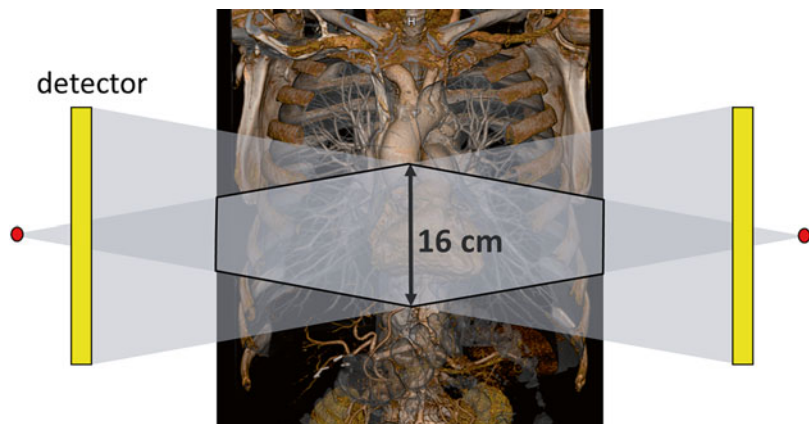
2.2 CT Systems with Area Detector

An area detector is a CT detector wide enough in the through-plane (z -axis) direction to cover entire organs, such as the heart, the kidneys, or the brain, in one axial scan without table movement. Two commercially available CT systems provide 16 cm detector coverage at isocenter, either with a collimation of 320×0.5 mm and 0.27 s rotation time (Aquilion ONE, Toshiba Medical Systems, Japan) or with 256×0.625 mm and 0.28 s rotation time (Revolution, GE Healthcare, USA). The SFOV is cone shaped in the z -axis direction (see Fig. 8).

CT scanners with area detectors are optimized for axial scanning without table movement – this scan technique has benefits in ECG-controlled cardiac imaging and in the acquisition of dynamic CT data, e.g., of the brain. Larger scan volumes in the z -direction, e.g., the entire thorax, have to be covered by “stitching,” i.e., by appending axial scans shifted in the z -direction. With increasing SFOV, more overlap in the z -direction is required for gapless volume coverage. Another option is standard spiral scanning. Then, however, only a smaller detector coverage of, e.g., 80 mm is typically available because of image reconstruction challenges, and the maximum table feed is limited to, e.g., 300 mm/s.

In ECG-controlled cardiac CT imaging, an image stack with an anatomical coverage corresponding to the detector z -width is acquired in each heartbeat. Typical MDCT detectors provide a z -coverage of 40 mm (and recently up to 80 mm) at isocenter, so two to four of these image stacks acquired in two to four consecutive heartbeats have to be put together to a volume image of the heart (Flohr et al. 2007). These image stacks can be blurred or shifted relative to each other as a consequence of insufficient temporal resolution or variations of the heart motion from one cardiac cycle to the next, resulting in stair-step or banding artifacts. CT systems with 16 cm detector coverage avoid these artifacts, because they can scan the entire heart in one axial scan without table movement (Rybicki et al. 2008). As a downside, all images will be affected in case of arrhythmia or ectopic beats during data acquisition. Another challenge of larger detectors is increased x-ray scatter. Scattered radiation may cause hypodense cupping or streaking artifacts, and the scatter-induced noise may reduce the contrast-to noise-ratio (CNR) in the images (Flohr et al. 2009a). Meanwhile, successful use of CT systems with 16 cm detector coverage for coronary CTA and other cardiac applications has been demonstrated (Rybicki et al. 2008; Steigner et al. 2009; Dewey et al. 2009). The application spectrum has been extended to, e.g., scanning of patients with atrial fibrillation (Kondo et al. 2013)

Fig. 8 Schematic illustration of axial CT scanning with a CT system with an area detector wide enough to cover entire organs such as the heart. Two commercially available CT systems provide 16 cm z -coverage at isocenter



and coronary CTA combined with the first-pass perfusion evaluation (George et al. 2015; Sharma et al. 2015). The second generation of 320-row CT scanners has been shown to enable coronary CTA at reduced radiation dose compared to the first generation (Tomizawa et al. 2013; Chen et al. 2013).

As a second benefit, CT systems with area detectors can acquire dynamic volume data by repeatedly scanning the same anatomical range without table movement. This is useful in dynamic CT angiographic examinations, e.g., in patients with brain arteriovenous malformations (Willems et al. 2012) or in volume perfusion studies, e.g., of the brain (Manniesing et al. 2016). In the context of thoracic scanning, 320-detector row first-pass perfusion scanning has been used to differentiate between malignant and benign pulmonary nodules (Ohno et al. 2011).

In triple-rule-out acute chest pain evaluation, the use of the sequential wide-volume mode proved to be more dose efficient than standard spiral scanning (Kang et al. 2012).

2.3 Dual-Source CT

A dual-source CT (DSCT) is a CT system with two x-ray tubes and two detectors at an angle of about 90° (see Fig. 9). Both measurement systems acquire CT scan data simultaneously at the same anatomical level of the patient (same z-position).

The first generation of DSCT scanners with 2×64 slices and 0.33 s gantry rotation time was introduced in 2006 (Somatom Definition, Siemens Healthcare, Forchheim, Germany), the second generation with 2×128 slices and 0.28 s gantry rotation time in 2009 (Somatom Definition Flash, Siemens Healthcare, Forchheim, Germany), and the third generation with 2×192 slices and 0.25 s gantry rotation time in 2014 (Somatom Definition Force, Siemens Healthcare, Forchheim, Germany).

DSCT systems provide significantly improved temporal resolution for cardiothoracic imaging. The shortest data acquisition time for an image corresponds to a quarter of the gantry rotation time. Close to the isocenter, 180° of scan data is

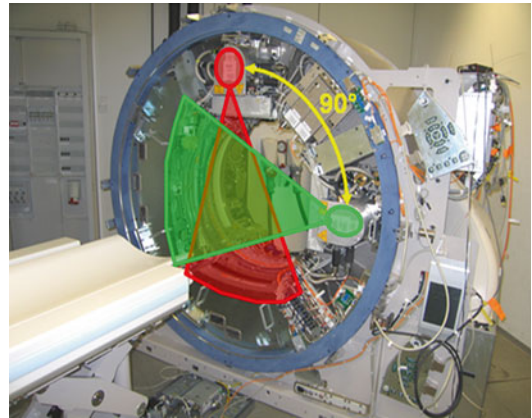


Fig. 9 DSCT with two independent measurement systems. The image shows the first-generation DSCT with an angle of 90° between both measurement systems. To increase the SFOV of detector B, a larger system angle of 95° was chosen for the second and third generations

the minimum needed for image reconstruction. Due to the 90° angle between both x-ray tubes, each of the measurement systems needs to acquire only 90° of scan data. The two 90° segments at the same anatomical level are put together to the 180° scan. Using this technique, a temporal resolution of 83, 75, and 66 ms, respectively, is achieved for the three generations of DSCT systems. With the dual-source approach, temporal resolution is independent of the patient's heart rate, because data from one cardiac cycle only are used to reconstruct an image. This is a major difference to single-source MDCT systems, which can provide similar temporal resolution by combining data from several heart cycles to an image in a multi-segment reconstruction. Then, however, temporal resolution strongly depends on the relation of heart rate and gantry rotation time. Meanwhile, several clinical studies have demonstrated the potential of DSCT to reliably perform coronary CT angiographic studies in patients with high and even irregular heart rates (e.g., Sun et al. 2011; Lee et al. 2012; Paul et al. 2013). DSCT is sufficiently accurate to diagnose clinically significant coronary artery disease in some or all difficult to image patients (Westwood et al. 2013). The good temporal resolution is also beneficial to reduce motion artifacts in cardiothoracic studies (e.g., Hutt et al. 2016).

With a DSCT system, both x-ray tubes can be operated at different kV settings, e.g., 80 and 140 kV, to acquire dual-energy CT data. The advantages and disadvantages of different techniques to acquire dual-energy CT data as well as clinically relevant applications will be discussed in Sect. 4.

While the maximum spiral pitch in single-source CT images is limited to about 1.5 to ensure gapless volume coverage, DSCT systems can be operated at double the pitch. Data acquired with the second measurement system, a quarter rotation after the first measurement system can be used to fill the sampling gaps up to a pitch of about 3.2 in a limited SFOV that is covered by both detectors (Petersilka et al. 2008; Flohr et al. 2009b). At maximum pitch, no redundant data are acquired, and a quarter rotation of data per measurement system is used for image reconstruction. Temporal resolution is then a quarter of the gantry rotation time. At decreasing pitch, temporal resolution worsens because of the increasing angular data segment that corresponds to an image. At a pitch of 2, as an example, temporal resolution is about 0.4 times the rotation time – this is 100 ms with the third-generation DSCT (Flohr et al. 2009b).

With the high-pitch scan mode, very high scan speed is achieved – up to 450 mm/s with the second-generation DSCT (38.4 mm detector coverage, 0.28 s gantry rotation time) and up to 737 mm/s with the third-generation DSCT (57.6 mm detector coverage, 0.25 s gantry rotation time). This is beneficial for the examination of larger anatomical ranges in very short scan times, e.g., for chest CTA at high temporal resolution (Tacelli et al. 2010), for the evaluation of pulmonary embolism and visualization of most cardiac structures and proximal coronary arteries (Hou et al. 2013), for fast CTA scans of the aorta at low radiation and contrast doses (Apfaltrer et al. 2012), or when the patient has limited ability to cooperate, such as in pediatric radiology (Lell et al. 2011; Bridoux et al. 2015) (see Fig. 10).

The high-pitch scan mode can also be used in combination with ECG triggering – the patient's ECG triggers both table motion and data acquisition. The patient table is positioned, and table acceleration is started in a way that the table arrives at the prescribed start z-position (e.g., the base or the apex of the heart) at the requested cardiac phase after full table speed has been reached (see Fig. 11). Then data acquisition begins.

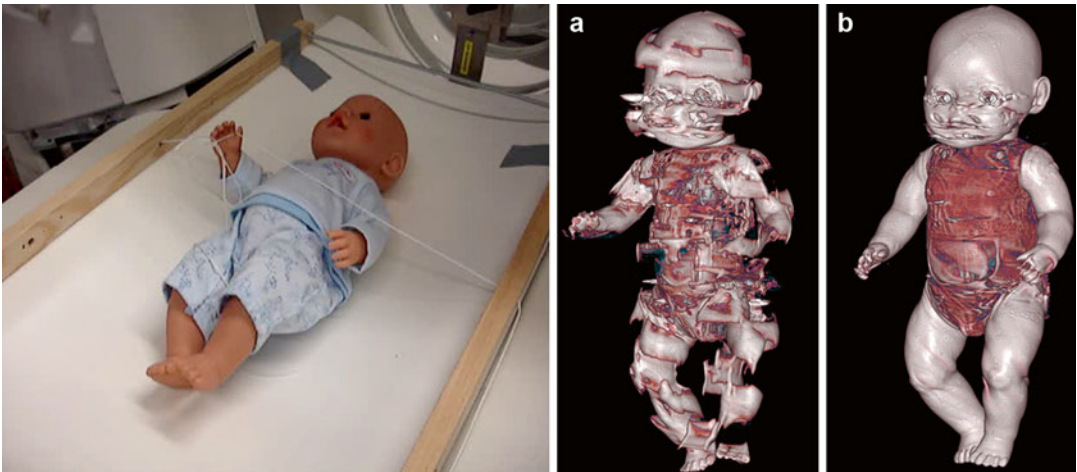
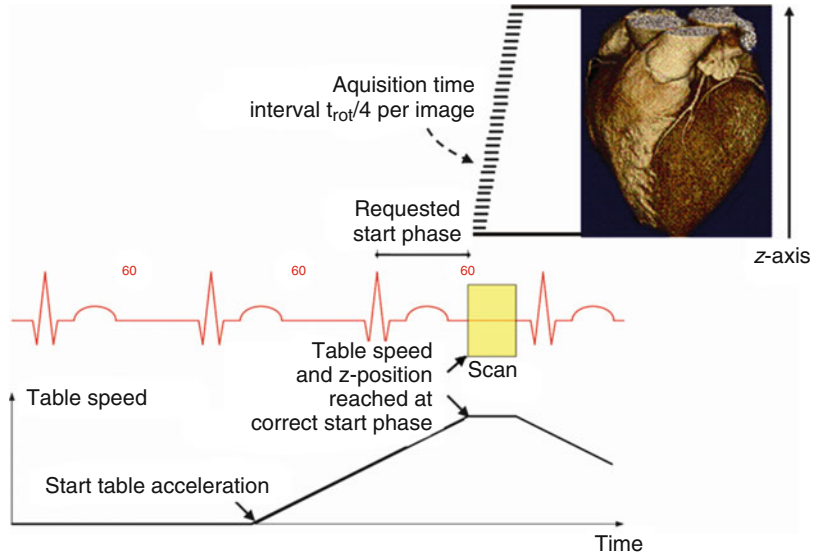


Fig. 10 CT scans of a moving doll phantom simulating motion of a child without sedation. (a) VRT of the phantom scanned with a standard spiral (pitch 1, 0.33 s rotation time) shows significant motion artifacts. (b) Using the high-pitch spiral (pitch 3.2, 0.33 s rotation time) motion

artifacts are significantly reduced because of the very short scan time and the good temporal resolution per image (Courtesy of C. McCollough, Clinical Innovation Center, Mayo Clinic Rochester, Mn, USA)

Fig. 11 ECG-triggered start of table movement and data acquisition for the high-pitch DSCT spiral



The scan data for images at adjacent z -positions are acquired at slightly different phases of the cardiac cycle. Meanwhile, several clinical studies have demonstrated the successful use of the high-pitch scan technique for coronary CT angiography in patients with sufficiently low and stable heart rate (<65 bpm with the second-generation DSCT, <73–75 bpm with the third-generation DSCT), with the potential to scan the entire heart in one beat at very low radiation dose (Achenbach et al. 2009; Lell et al. 2009; Leschka et al. 2009, Gordic et al. 2014a, Morsbach et al. 2014).

ECG-triggered high-pitch scans can be used for comprehensive thorax examinations in the emergency room and in the planning of TAVR procedures, because they provide adequate visualization of the coronary arteries, the aorta, and the iliac arteries in one scan at low radiation dose. The very short total scan time may potentially allow for a reduction of the amount of contrast agent (see, e.g., Wuest et al. 2012; Azzalini et al. 2014). Figure 12 shows an ECG-triggered high-pitch CTA of the aorta as an example.

Despite their clinical benefits, DSCT systems have to cope with some challenges. One challenge is the presence of cross-scattered radiation, i.e., scattered radiation from x-ray tube B detected by detector A and vice versa. Cross-scattered radiation – if not corrected

for – can result in image artifacts and degraded CNR of the images (Petersilka et al. 2010). Another challenge is the limited SFOV of the second detector, which was increased from 25 cm in the first-generation DSCT to 35.5 cm in the third-generation DSCT.

3 Radiation Dose Reduction

3.1 Low-kV Scanning

Most CT scans are performed with the use of iodinated contrast agent. The x-ray attenuation of iodine and as a consequence, its CT number in a CT image increases with decreasing mean energy of the x-ray beam, i.e., with the use of lower x-ray tube voltages (kV) (see, e.g., McCollough et al. 2009). This behavior is caused by the k-edge of iodine at 33 keV. The x-ray attenuation of soft tissue depends only very weakly on the x-ray tube voltage. Therefore, the image contrast of tissues and vessels that take up iodinated contrast agent increases relative to other surrounding tissues at lower x-ray tube voltage. If the same radiation dose is applied to the patient when using lower kV, the increased contrast of iodine in the image translates into increased iodine contrast-to-noise ratio (CNR) (see Fig. 13).



Fig. 12 ECG-triggered high-pitch spiral scan of the aorta and the iliac arteries in a patient with aortic dissection. Scan parameters: 0.25 s rotation time, pitch 3.2, 90 kV, DLP=177 mGy cm. Total scan time 0.8 s. Note the clear visualization of the right coronary artery (Courtesy of Klinikum Großhadern, Munich, Germany)

The increased CNR at lower x-ray tube voltage may either be exploited to reduce the radiation dose to the patient or to reduce the amount of iodinated contrast agent.

Unfortunately, with decreasing x-ray tube voltage, the tube current–time product mAs has to be significantly increased to provide adequate radiation dose in particular for larger patients. Because of missing tube power reserves, low-kV imaging has been mainly used for children and small patients. Meanwhile, new technologies are

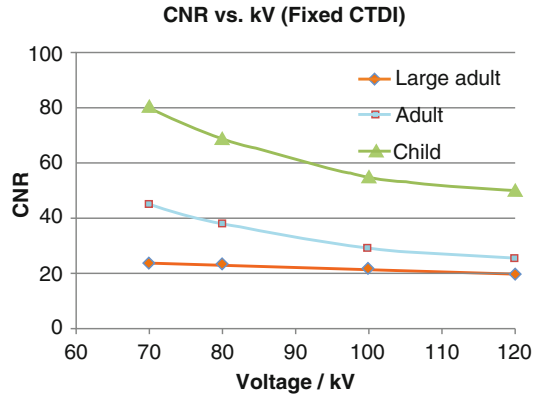


Fig. 13 Iodine contrast-to-noise ratio (CNR) at equal radiation dose (*equal CTDI*) as a function of the x-ray tube voltage (*kV*) for phantoms representing the attenuation of children, adults, and large adults, on a second-generation DSCT. A small tube filled with diluted iodine solution was placed at the center of the phantoms; the iodine concentration was chosen to provide the typical contrast of the aorta in a CT angiographic examination. Note the increase of the CNR with decreasing x-ray tube voltage

available that automatically adapt the x-ray tube voltage to the size and shape of the patient and the planned examination, taking into account the tube power reserves of the respective CT system (e.g., CAREkV, Siemens Healthcare, Forchheim, Germany). According to Niemann et al. (2013), automatic tube voltage selection reduced the radiation dose delivered during chest CT angiograms by 38.5% compared to the standard 120 kV protocol while improving the CNR of the examinations.

Recently, new x-ray tubes with significantly increased mA reserves and significantly increased power at low kV were introduced (VECTRON, Siemens Healthcare, Forchheim, Germany), which have the potential to extend low-kV scanning at reduced radiation dose and/or reduced contrast dose also to adult and obese patients (Meyer et al. 2014; Meinel et al. 2014). Meyer et al. (2014) observed that coronary CTA with a third-generation DSCT at 70 kV resulted in up to 52% lower radiation dose as well as up to 45% less contrast medium volume in nonobese adults (see Fig. 14 as an example).

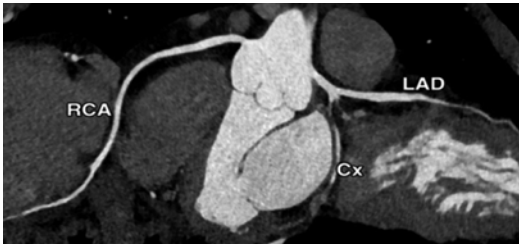


Fig. 14 Coronary CTA in an adult patient at 70 kV. ECG-triggered high-pitch scan at 64 bpm. Total radiation dose 0.21 mSv (Courtesy of Mannheim University Hospital, Germany)

3.2 Spectral Shaping

In CT examinations of the lung without contrast agent, spectral shaping may be used to significantly reduce the radiation dose to the patient. A tin filter, which can be moved into the x-ray beam in the pre-patient tube collimator box if needed, removes lower-energy x-ray photons from the x-ray spectrum and hardens it— these photons would otherwise mainly be absorbed in the patient without contributing to the image and would degrade the dose efficiency of the CT scan¹. Third-generation DSCT systems are equipped with 0.6 mm thick tin filters, which can be used with 100 or 150 kV x-ray tube voltage. Figure 15 demonstrates the effect of the tin filter on the shape of the spectra for 100 kV + tin filter (100 Sn kV) and 150 kV + tin filter (150 Sn kV). The novel scan mode offers a potential radiation dose reduction in non-enhanced lung examinations compared to standard 120 kV scans.

Gordic et al. (2014b) evaluated the image quality and sensitivity of low-dose CT with spectral shaping and iterative reconstruction for the detection of pulmonary nodules in a phantom setting. They concluded that radiation dose levels of non-enhanced chest CT for the detection of pulmonary nodules can be lowered down

¹Please note that this is valid for non-contrast scans. In contrast-enhanced examinations, the increased x-ray absorption of iodine at lower energies overcompensates this effect.

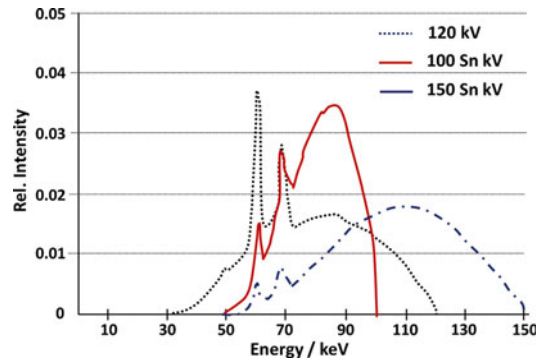


Fig. 15 Spectral shaping by Sn (tin) pre-filtration. Standard 120 kV spectrum as compared to 100 and 150 Sn kV. The tin filter removes x-ray quanta at lower energies (lower keV) from the spectra. Note the onset of the tin-filtered spectra at about 50 keV as compared to about 30 keV for the standard 120 kV spectrum and the very narrow, almost “mono-energetic” shape of the 100 Sn kV spectrum

to a level of 0.06 mSv when using 100 kV with tin pre-filtration in combination with advanced iterative reconstruction techniques. Image quality remains diagnostic and sensitivity remains high. This is potentially interesting for the use of CT in the context of lung cancer screening. According to Newell et al. 2015, quantitative CT lung imaging can be performed with spectral shaping and third-generation iterative reconstruction methods with acceptable image noise at very low-dose levels of 0.15 mGy (corresponding to about 0.07 mSv for a scan range of 350 mm). It remains subject of further studies how well subtle features of the lung parenchyma can be evaluated at such a low radiation dose. Figure 16 shows a representative example of a non-enhanced thorax scan with spectral shaping (100 Sn kV) at a radiation dose of 0.07 mSv.

3.3 Iterative Reconstruction

As an add-on to the dose reduction approaches described above, iterative image reconstruction has found its way into routine CT scanning after it had been proposed in 2007 as a method to improve image quality, enhance image resolution, and lower image noise in CT (Thibault et al. 2007).

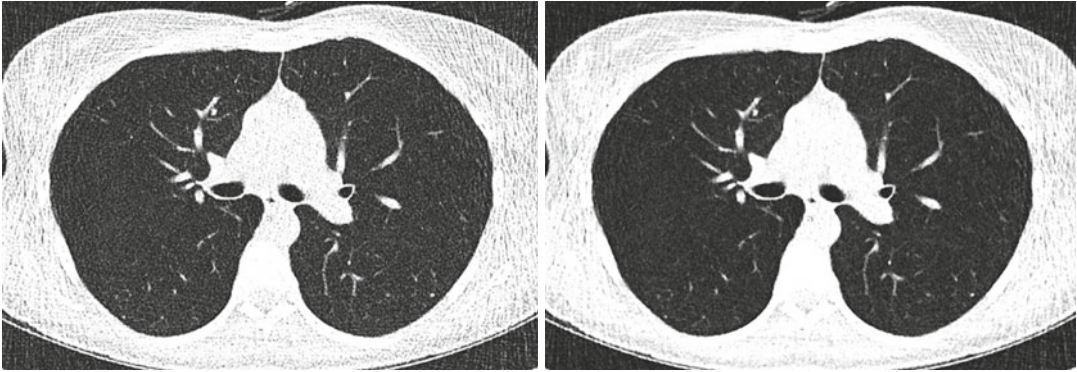


Fig. 16 Non-enhanced lung image acquired with spectral shaping (100 Sn kV) and two levels of iterative reconstruction (ADMIRE level 3, *left*, and level 5, *right*) at a

radiation dose of 0.07 mSv (Courtesy of Universitätsspital Zürich, Switzerland)

While increased spatial resolution is directly correlated with increased image noise in filtered back projection, the standard image reconstruction approach in all medical CT scanners today, it is to a certain extent decoupled from image noise in an iterative reconstruction.

With iterative reconstruction, a correction loop is introduced into the image reconstruction process (Thibault et al. 2007). After an image has been reconstructed from the measured projection data, synthetic projections are calculated from that image by ray tracing. Because image reconstruction is not exact, the synthetic projections are not fully identical to the measured projections. The deviation is used to reconstruct a correction image and update the original image in an iterative loop. Each time the image is updated, nonlinear image processing is used to stabilize the solution. It maintains or enhances spatial resolution at higher object contrasts and reduces image noise in low-contrast areas. This step, called regularization, is essential for the image noise reduction claimed with most iterative reconstruction approaches. The repeated calculation of correction projections mainly removes image artifacts introduced by the approximate nature of the filtered back projection reconstruction when applied to multi-row CT data. In some approaches, a statistical raw-data weighting is added in the reconstruction loops which assigns low weights to measured raw data with high noise. This step reduces image noise in particular

in low-dose situations, but at the expense of a certain loss of spatial resolution.

There is a variety of different iterative reconstruction techniques commercially available, such as ASIR, VEO and ASIR-V (GE Healthcare, USA), IRIS, SAFIRE and ADMIRE (Siemens Healthcare, Forchheim, Germany), iDose (Philips), and AIDR3D (Toshiba). While the technical realization is highly vendor specific, using some or all of the steps described above, all approaches aim at including the statistical properties of the acquired measurement data into the image reconstruction process in a better way than traditional filtered back projection.

The reduced image noise in low-contrast areas is the prerequisite for a potential radiation dose reduction, which is the main goal when using iterative reconstruction. Iterative reconstruction has been widely used for chest CT examinations (see Fig. 16), and a potential for substantial radiation dose reduction has been reported (see, e.g., Kim et al. 2015; Wang et al. 2015; Pontana et al. 2011a, b, 2015; Padole et al. 2014; Vardhanabuthi et al. 2013). By analyzing 24 studies using iterative reconstruction for chest CT, den Harder et al. (den Harder et al. 2015) found that by means of iterative reconstruction, radiation dose can be reduced to less than 2 mSv for contrast-enhanced chest CT, while non-contrast-enhanced chest CT is possible at a sub-mSv dose.

However, as a downside, it has also been shown that iterative reconstruction may alter

both the qualitative and quantitative assessment of smoking-related lung disease (Hague et al. 2014) and may affect quantitative CT measures in the assessment of emphysema and air trapping and should therefore be used with caution (Mets et al. 2012).

4 Dual-Energy CT (DECT)

CT imaging shows the patient's anatomy; however, it cannot provide information about the chemical composition of the examined structures. CT is only sensitive to the x-ray attenuation coefficients μ of the examined objects. Tissues of different chemical composition but with the same μ will appear with the same Hounsfield number in the CT image. Additional information obtained by measurements at different x-ray energies E can help overcome this limitation. Alvarez and Macovski observed that in the typical energy range of the CT x-ray spectra, ranging from 30 to 140 keV, only two absorption processes are relevant, the Compton effect and the photoelectric effect (Alvarez and Macovski 1976). Both have a characteristic energy dependence which is almost independent of the atomic number Z . As a consequence, all materials in the examined scan volume can be decomposed into two different base materials, e.g., water and bone or water and iodine. The relative contributions of these two base materials to each voxel of interest can be determined if the x-ray absorption by the object of interest is measured with two different spectra. In some cases, by observing a volume conservation constraint, decomposition into three materials is possible, e.g., water, bone, and iodine. Because there are only two different absorption mechanisms, however, it is not possible to e.g., separate N different materials by measurements at N different energies.

4.1 Instrumentation

There are several methods to acquire CT data with spectral information. In single-source CT systems, the kV setting of the x-ray tube can be

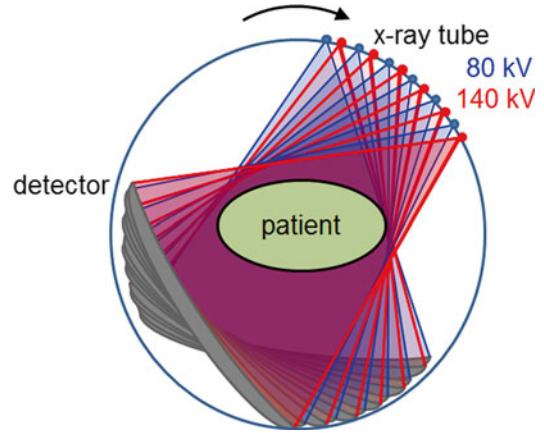


Fig. 17 Schematic drawing illustrating the principle of dual-energy CT data acquisition by means of fast kV switching. The x-ray tube voltage is rapidly switched from 80 to 140 kV and vice versa between two projections

changed either between different CT scans (slow kV switching) or more rapidly between the different projections of a CT scan (fast kV switching (see Fig. 17)). Slow kV switching is problematic for chest imaging because cardiac motion causes registration problems between the two data sets acquired at different kV.

Fast kV switching, usually between 80 and 140 kV, is per se well suited for thoracic imaging because of the nearly simultaneous acquisition of low-energy and high-energy projections which avoids registration problems and allows the use of raw-data-based dual-energy algorithms. Fast kV switching was commercially reintroduced in 2009 (Gemstone Spectral Imaging, GE Healthcare, USA) (see, e.g., Zhang et al. 2011). As a downside, current tube technology doesn't allow switching the tube current between two projections. Equal radiation dose at 80 and 140 kV can only be achieved if each 80 kV projection is two–four times longer than the corresponding 140 kV projection. This reduces the number of projections per rotation and may cause sampling artifacts in the images. Another drawback is the fixed and relatively high tube current that is required to obtain stable switching between both tube potentials, which prevents the use of anatomical dose modulation

techniques to adapt radiation dose to the patient's size and shape.

Dual-layer detectors consisting of two conventional scintillation detectors on top of each other enable the acquisition of spectral CT data with a single polychromatic x-ray spectrum and without further modifications of the CT system. A CT scanner with dual-layer detector was commercially introduced in 2013 (IQon, Philips Healthcare, the Netherlands). Dual-layer detectors enable the acquisition of dual-energy data in the full SFOV and with perfect registration between the high- and low-energy data. However, spectral separation is not as good as with the use of two different x-ray spectra (Tkaczyk et al. 2007).

Another alternative for dual-energy data acquisition is the use of dual-source CT systems, which have the potential to acquire DE data by operating both x-rays tubes at different kV settings. The scan parameters can be individually adjusted for both measurement systems, resulting in a flexible choice of scan protocols. In combination with online anatomical dose modulation (CAREDose 4D, Siemens Healthcare, Forchheim, Germany), the radiation dose to the patient can be fine-tuned to patient's size and the planned examination. As a drawback, DE data acquisition is limited to a smaller, central FOV covered by both detectors. Cross-scattered radiation has to be carefully corrected for in order not to degrade the stability of the Hounsfield numbers and – as a consequence – the quality of the image-based DE evaluation. Furthermore, images of moving objects may show slightly different motion artifacts due to the 90° offset between both measurement systems, which may result in registration problems affecting material decomposition. In practice, however, this problem is mitigated by the good temporal resolution of DSCT and – if necessary – by nonrigid image registration.

The quality of dual-energy CT examinations relies on the effective separation of the energy spectra. More spectral overlap and worse energy separation mean less efficient and less precise tissue differentiation, which has to be compensated by increased radiation dose. With

DSCT systems spectral separation can be optimized by introducing additional pre-filtration into the high-kV beam, e.g., by means of a filter that can be moved in when needed and moved out for non-DE applications. In the second-generation and third-generation DSCT systems, additional tin filters (Sn) with a thickness of 0.4 mm (second-generation DSCT) and 0.6 mm (third-generation DSCT) are used. They shift the mean energy of the 140 kV spectrum and the 150 kV spectrum (third-generation DSCT) to higher values, which increases spectral separation (see Fig. 18).

Spectral pre-filtration of the high-kV beam is beneficial for DECT at low radiation dose. Several authors have meanwhile demonstrated dual-source DECT scanning with no dose penalty compared to standard single-energy CT. Schenzle et al. (2010) report the feasibility of dual-source DECT without increasing radiation dose in chest CT. Bauer et al. (2011) compare radiation dose and image quality of 64-slice CT and dual-source DECT for CT pulmonary angiography (CTPA). They conclude that the use of the second-generation DECT in 80/140 Sn kV configuration allows for significant dose reduction with image quality similar to 120 kV CTPA. A comprehensive overview on radiation dose in DECT can be found in (Henzler et al. 2012).

4.2 Applications

For thoracic DECT, dedicated scan protocols are available that aim at high scan speed and good temporal resolution by using fast gantry rotation (e.g., 0.28 or 0.25 s). For dedicated cardiac examinations, both ECG-triggered DE sequential “step-and-shoot” scanning and ECG-gated DE spiral scanning are provided, both at the fastest gantry rotation speed of the respective CT scanner.

Clinically relevant applications for thoracic and cardiothoracic scanning are the computation of pseudo mono-energetic images or iodine distribution maps of the lung parenchyma as a surrogate of the local blood volume and lung perfusion

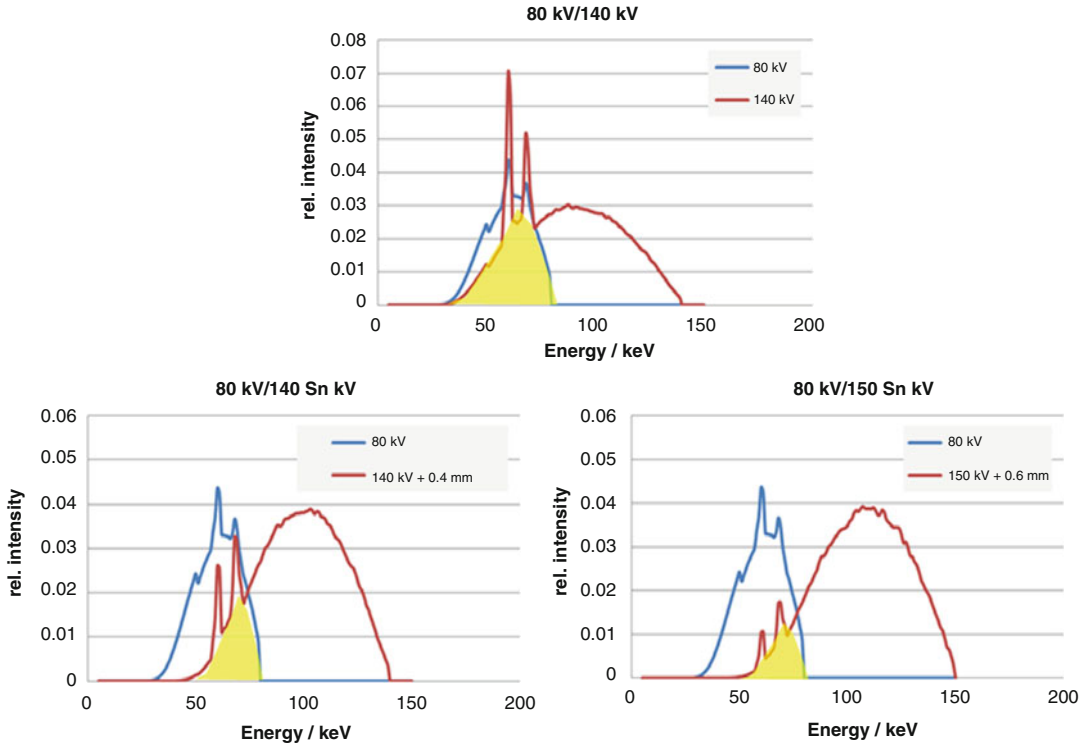


Fig. 18 *Top:* Standard 80 and 140 kV spectra. The mean energy is 69 keV for the 140 kV spectrum and 52 keV for the 80 kV spectrum. Both spectra overlap significantly (indicated in yellow). *Bottom left:* Standard 80 kV spectrum and 140 kV spectrum with additional 0.4 mm tin pre-

filtration. Note the shift of the 140 kV spectrum to higher energies. The mean energy is now 89 keV. *Bottom right:* Standard 80 kV spectrum and 150 kV spectrum with additional 0.6 mm tin pre-filtration. Note the further reduced spectral overlap

Pseudo mono-energetic images at arbitrary energies can be obtained from the polychromatic low-kV and high-kV images, if we assume that the object consists of only two base materials in variable concentrations, e.g., water (soft tissue) and iodine. The concentrations of both materials in each image pixel are calculated by means of an image-based material decomposition. They are multiplied with predicted CT numbers per concentration at the desired energy and summed up to the final mono-energetic image. Other materials will contribute to both base material images, their CT numbers may therefore not reflect the actual enhancement of the respective material at the desired energy.

Pseudo mono-energetic images may be used to benefit from the increased iodine contrast at lower keV in CT angiographic studies. With conventional decomposition approaches, optimum CNR in contrast-enhanced thoracic scans has

been observed at 60 keV for the aorta, pulmonary arteries, and veins. For the superior vena cava and brachiocephalic veins, the reconstructions at 100 keV with reduced iodine contrast enabled reduction of beam-hardening artifacts (Delesalle et al. 2013).

Performance can be improved by means of recently introduced algorithms (e.g., mono+, Siemens Healthcare, Forchheim, Germany) that efficiently reduce image noise at low and high keV (Grant et al. 2014). Using these techniques, images at the target keV and images at optimal keV from a noise perspective (typically, minimum image noise is obtained at approximately 70 keV) are computed. For the final images, the lower spatial frequencies (that contain most of the object structure) from the images at the target keV are combined with the higher spatial frequencies (that contain most of the image noise) from the images at optimal keV from a

noise perspective. It has been shown (Grant et al. 2014) that use of the mono+–technique at 40 keV may be more efficient to optimize iodine CNR than low-kV scans, which has been the established and recommended method to improve iodine CNR to date (see also Fig. 19). Recent publications demonstrated that mono+ images at 40 keV improve the contrast of dual-energy CT pulmonary angiography (Meier et al. 2015). Figure 20 shows a clinical example for illustration.

The polychromatic low-kV and high-kV images can also be used for the subtraction of iodine from a contrast-enhanced CT scan, to compute both a virtual non-enhanced CT image and an iodine map showing the iodine content per image pixel. In lung imaging, the iodine content is a surrogate parameter for the perfused blood volume in the lung parenchyma or in lung tumors. The underlying technique is a modified three-material decomposition. In a diagram showing the CT number of each image pixel at low kV as a function of its CT number at high kV, image pixels containing mixtures of air and soft tissue (these are the relevant two “base materials” in lung imaging) are located along a line between

air and soft tissue (see Fig. 21). If iodine is added, the respective data points in the CT-number diagram move in the direction of the iodine enhancement vector. To extract the iodine, each pixel is projected onto the line between air and soft tissue along the direction of the iodine enhancement vector. The length of the displacement vector represents the enhancement attributed to iodine in that pixel (see the two examples “Pixel 1” and “Pixel 2” in Fig. 21). The iodine map can provide quantitative information about the iodine content in mg/ml.

Iodine maps have been frequently used in patients with pulmonary embolism to assess perfusion defects, which show up as hypodense areas with reduced iodine content (see, e.g., Pontana et al. 2008; Thieme et al. 2008, 2009; Ferda et al. 2009). Figure 22 shows a clinical example.

Dual-energy CT of the lung has also other clinical applications, such as the evaluation of regional perfusion according to the presence of emphysematous changes in the lung parenchyma in patients with chronic obstructive pulmonary disease (Remy-Jardin and Remy 2008), the depiction of regional alterations of lung perfusion in

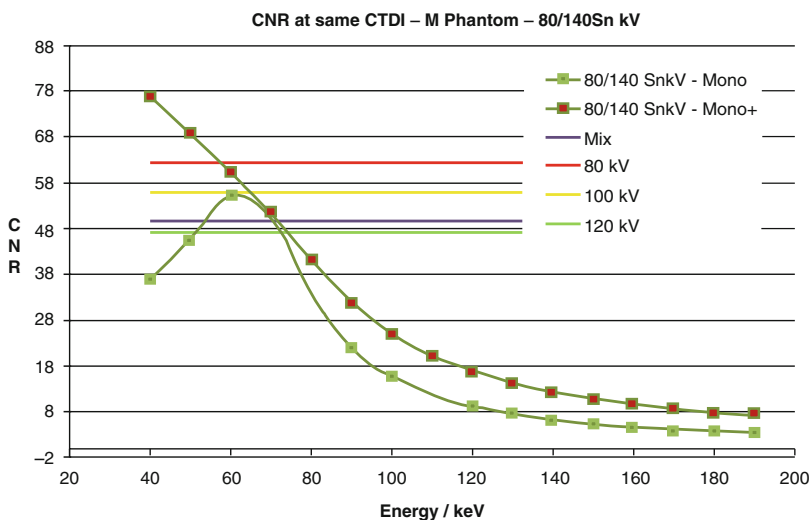


Fig. 19 Iodine CNR as a function of the energy (in keV) of pseudo mono-energetic images computed with a standard two-material decomposition (mono) and with an advanced algorithm (mono+). In addition, CNRs from single-energy scans (at 80, 100 and 140 kV) for the same

medium-sized body phantom at the same radiation dose are shown (From (Grant et al. 2014)). Note the better iodine CNR with mono+ even compared with 80 kV scans in the energy range 40–50 keV

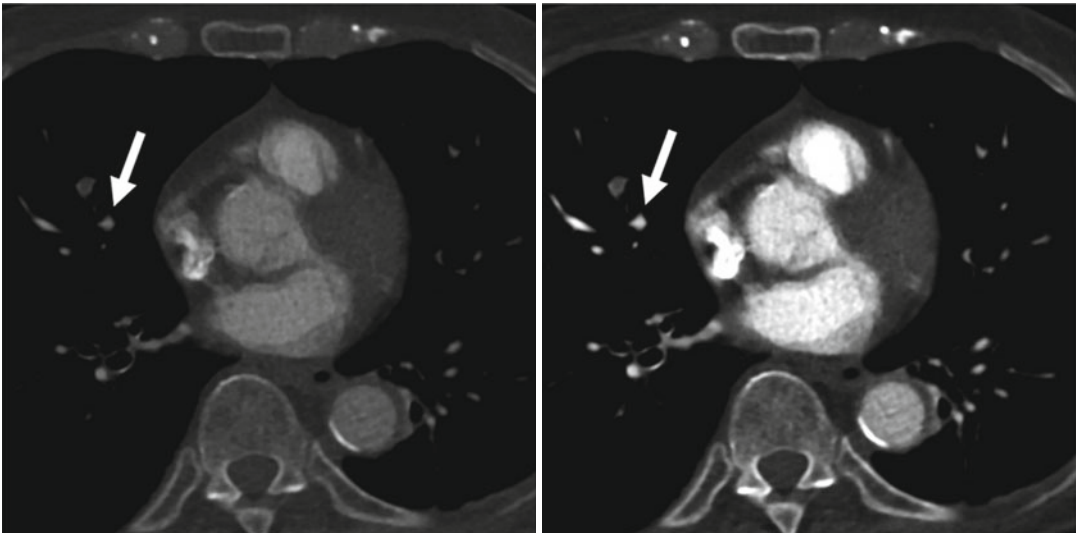
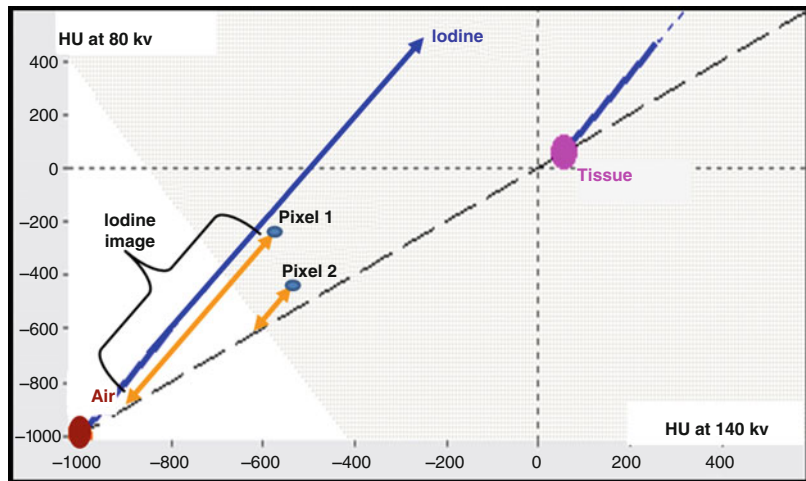


Fig. 20 Image example from a DE pulmonary CTA examination. *Left:* In the standard mixed image (corresponding to a 120 kV scan), opacification of peripheral pulmonary arteries is suboptimal (*arrow*), and the examination is of limited diagnostic value. *Right:* Reconstruction

of pseudo mono-energetic images at 40 keV with an advanced algorithm (mono+) demonstrates increased iodine contrast and allows for a reliable exclusion of PE (Adapted from (Meier et al. 2015))

Fig. 21 Principle of a modified three-material decomposition: subtraction of iodine from contrast-enhanced DECT images to compute both an iodine map (“iodine image”) and a virtual non-enhanced image



smokers with predominant emphysema (Pansini et al. 2009), or the characterization of lung tumors (Aoki et al. 2014; Wang et al. 2014). According to Lu et al., (2012) dual-energy CT of the lung can improve the diagnosis of acute and chronic PEs, other vascular disorders, lung malignancies, and parenchymal diseases.

In xenon lung ventilation studies, dual-energy CT allows extracting the amount of inhaled xenon gas per voxel without the need for a pre-

scan without xenon. Hence, limitations in the quantification of Xe enhancement by ventilation mismatch, i.e., by the variability of lung attenuation caused by different lung volumes between scans, can be avoided.

With ongoing technical refinements, DECT has the potential to provide complementary information in a variety of chest disorders. An overview of dual-energy imaging of the thorax is, e.g., available in (Lu et al. 2012) or (Remy-Jardin et al. 2014).

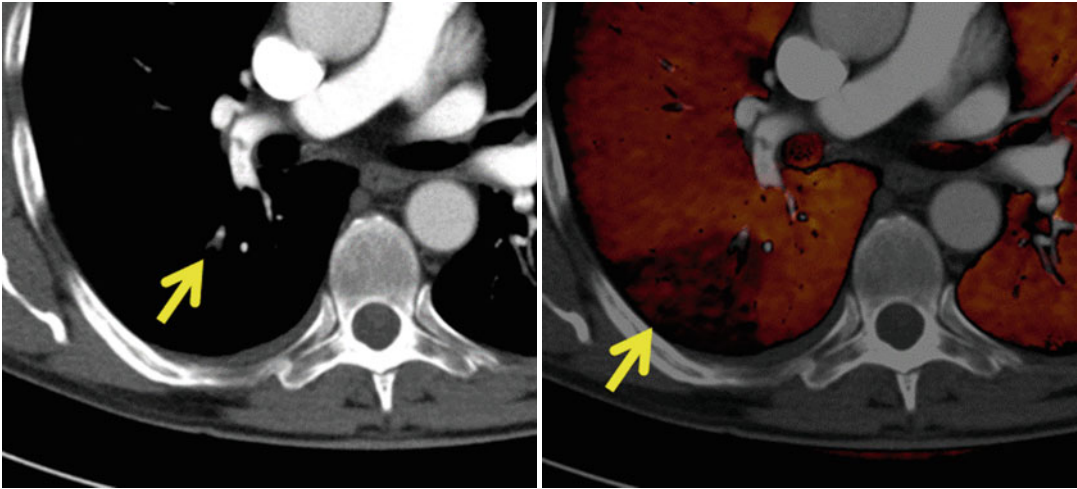


Fig. 22 Visualization of perfusion defects in the lung parenchyma caused by pulmonary embolism. DECT angiography using a second-generation DSCT, scan parameters 80 kV/140 Sn kV, rotation time 0.28 s. *Left:* Mixed low-kV/high-kV axial image corresponding to a standard 120 kV image shows small embolus that

occludes a sub-segmental vessel in the right lower lobe (*arrow*). *Right:* DE iodine map of the lung parenchyma as a colored overlay (*red*) shows the corresponding typical wedge-shaped perfusion defect (*dark zone, arrow*) (Courtesy of Klinikum Großhadern, Munich, Germany)

References

- Achenbach S, Marwan M, Schepis T, Pflederer T, Bruder H, Allmendinger T, Petersilka M, Anders K, Lell M, Kuettner A, Ropers D, Daniel WG, Flohr T (2009) High-pitch spiral acquisition: a new scan mode for coronary CT angiography. *J Cardiovasc Comput Tomogr* 3:117–121
- Achenbach S, Manolopoulos M, Schuhbäck A, Ropers D, Rixe J, Schneider C, Krombach GA, Uder M, Hamm C, Daniel WG, Lell M (2012) Influence of heart rate and phase of the cardiac cycle on the occurrence of motion artifact in dual-source CT angiography of the coronary arteries. *J Cardiovasc Comput Tomogr* 6(2):91–98
- Alvarez RE, Macovski A (1976) Energy-selective reconstructions in X-ray computerized tomography. *Phys Med Biol* 21(5):733–744
- Aoki M, Takai Y, Narita Y, Hirose K, Sato M, Akimoto H, Kawaguchi H, Hatayama Y, Miura H, Ono S (2014) 23. Correlation between tumor size and blood volume in lung tumors: a prospective study on dual-energy gemstone spectral CT imaging. *J Radiat Res* 55(5): 917–923
- Apfaltrer P, Hanna EL, Schoepf UJ, Spears JR, Schoenberg SO, Fink C, Vliegthart R (2012) Radiation dose and image quality at high-pitch CT angiography of the aorta: intraindividual and interindividual comparisons with conventional CT angiography. *AJR Am J Roentgenol* 199(6):1402–1409
- Azzalini L, Abbara S, Ghoshhajra BB (2014) Ultra-low contrast Computed Tomographic Angiography (CTA) with 20-mL total dose for Transcatheter Aortic Valve Implantation (TAVI) planning. *J Comput Assist Tomogr* 38(1):105–109
- Bauer RW, Kramer S, Renker M et al (2011) Dose and image quality at CT pulmonary angiography: comparison of first and second generation dual energy CT and 64-slice CT. *Eur Radiol* 21:2139–2147
- Baumueeller S, Winklehner A, Karlo C, Goetti R, Flohr T, Russi EW, Frauenfelder T, Alkadhi H (2012) Low-dose CT of the lung: potential value of iterative reconstructions. *Eur Radiol* 22(12):2597–2606
- Becker C, Knez A, Ohnesorge B, Schöpf U, Reiser M (2000) Imaging of non calcified coronary plaques using helical CT with retrospective EKG gating. *AJR* 175:423–424
- Beeres M, Schell B, Mastragelopoulos A, Herrmann E, Kerl JM, Gruber-Rouh T, Lee C, Siebenhandl P, Bodelle B, Zangos S, Vogl TJ, Jacobi V, Bauer RW (2012) High-pitch dual-source CT angiography of the whole aorta without ECG synchronisation: initial experience. *Eur Radiol* 22(1):129–137
- Bridoux A, Hutt A, Faivre JB, Flohr T, Duhamel A, Pagniez J, Remy J, Remy-Jardin M (2015) Coronary artery visibility in free-breathing young children on non-gated chest CT: impact of temporal resolution. *Pediatr Radiol* 45(12):1761–1770
- Bruzzi JF, Rémy-Jardin M, Delhaye D, Teisseire A, Khalil C, Rémy J (2006a) When, why, and how to examine the heart during thoracic CT: Part 1, basic principles. *AJR Am J Roentgenol* 186(2):324–332
- Bruzzi JF, Rémy-Jardin M, Delhaye D, Teisseire A, Khalil C, Rémy J (2006b) When, why, and how to examine the heart during thoracic CT: Part 2, clinical applications. *AJR Am J Roentgenol* 186(2):333–341

- Chen MY, Shanbhag SM, Arai AE (2013) Submillisievert median radiation dose for coronary angiography with a second-generation 320-detector row CT scanner in 107 consecutive patients. *Radiology* 267(1):76–85
- Coche E, Vlassenbroeck A, Roelants V, D'Hoore W, Verschuren F, Goncette L, Maldague B (2005) Evaluation of biventricular ejection fraction with ECG-gated 16-slice CT: preliminary findings in acute pulmonary embolism in comparison with radionuclide ventriculography. *Eur Radiol* 15:1432–1440
- Delesalle MA, Pontana F, Duhamel A, Faivre JB, Flohr T, Tacelli N, Remy J, Remy-Jardin M (2013) Spectral optimization of chest CT angiography with reduced iodine load: experience in 80 patients evaluated with dual-source, dual-energy CT. *Radiology* 267(1):256–266
- Delhay D, Remy-Jardin M, Salem R, Teisseire A, Khalil C, Delannoy-Deken V, Duhamel A, Remy J (2007) Coronary imaging quality in routine ECG-gated multidetector CT examinations of the entire thorax: preliminary experience with a 64-slice CT system in 133 patients. *Eur Radiol* 17(4):902–910
- den Harder AM, Willeminck MJ, de Ruitter QM, Schilham AM, Krestin GP, Leiner T, de Jong PA, Budde RP (2015) Achievable dose reduction using iterative reconstruction for chest computed tomography: a systematic review. *Eur J Radiol* 84(11):2307–2313
- Dewey M, Zimmermann E, Deissenrieder F, Laule M, Dübel HP, Schlattmann P, Knebel F, Rutsch W, Hamm B (2009) Noninvasive coronary angiography by 320-row computed tomography with lower radiation exposure and maintained diagnostic accuracy: comparison of results with cardiac catheterization in a head-to-head pilot investigation. *Circulation* 120(10):867–875
- Duan X, Wang J, Leng S, Schmidt B, Allmendinger T, Grant K, Flohr T, McCollough CH (2013) Electronic noise in CT detectors: impact on image noise and artifacts. *AJR Am J Roentgenol* 201(4):W626–W632
- Durand S, Paul JF (2014) Comparison of image quality between 70 kVp and 80 kVp: application to paediatric cardiac CT. *Eur Radiol* 24(12):3003–3009
- Ferda J, Ferdová E, Mírka H, Baxa J, Bednářová A, Flohr T, Schmidt B, Matějovič M, Kreuzberg B (2011). Pulmonary imaging using dual-energy CT, a role of the assessment of iodine and air distribution. *Eur J Radiol* 77(2):287–93
- Flohr T, Stierstorfer K, Bruder H, Simon J, Schaller S (2002a) New technical developments in multislice CT, part 1: approaching isotropic resolution with sub-mm 16-slice scanning. *Röfo Fortschr Geb Rontgenstr Neuen Bildgeb Verfahr* 174:839–845
- Flohr T, Bruder H, Stierstorfer K, Simon J, Schaller S, Ohnesorge B (2002b) New technical developments in multislice CT, part 2: sub-millimeter 16-slice scanning and increased gantry rotation speed for cardiac imaging. *Röfo Fortschr Geb Rontgenstr Neuen Bildgeb Verfahr* 174:1022–1027
- Flohr T, Stierstorfer K, Bruder H, Simon J, Polacin A, Schaller S (2003) Image reconstruction and image quality evaluation for a 16-slice CT scanner. *Med Phys* 30(5):832–884
- Flohr T, Stierstorfer K, Raupach R, Ulzheimer S, Bruder H (2004) Performance evaluation of a 64-slice CT-system with z-flying focal spot. *Röfo Fortschr Geb Rontgenstr Neuen Bildgeb Verfahr* 176:1803–1810
- Flohr TG, Stierstorfer K, Ulzheimer S, Bruder H, Primak AN, McCollough CH (2005) Image reconstruction and image quality evaluation for a 64-slice CT scanner with z-flying focal spot. *Med Phys* 32(8):2536–2547
- Flohr TG, McCollough CH, Bruder H, Petersilka M, Gruber K, Süß C, Grasruck M, Stierstorfer K, Krauss B, Raupach R, Primak AN, Küttner A, Achenbach S, Becker C, Kopp A, Ohnesorge BM (2006) First performance evaluation of a dual-source CT (DSCT) system. *Eur Radiol* 16(2):256–268
- Flohr T, Schoepf UJ, Ohnesorge B (2007) Chasing the heart – new developments for cardiac CT. *J Thorac Imag* 22(1):4–16
- Flohr TG, Raupach R, Bruder H (2009a) Cardiac CT: how much can temporal resolution, spatial resolution, and volume coverage be improved? *J Cardiovasc Comput Tomogr* 3(3):143–152
- Flohr TG, Leng S, Yu L, Allmendinger T, Bruder H, Petersilka M, Eusemann CD, Stierstorfer K, Schmidt B, McCollough C (2009) Dual-source spiral CT with pitch up to 3.2 and 75 ms temporal resolution: image reconstruction and assessment of image quality. *Med Phys* 36(12):5641–53.
- George RT, Mehra VC, Chen MY, Kitagawa K, Arbab-Zadeh A, Miller JM, Matheson MB, Vavere AL, Kofoed KF, Rochitte CE, Dewey M, Yaw TS, Niinuma H, Brenner W, Cox C, Clouse ME, Lima JA, Di Carli M (2015) Myocardial CT perfusion imaging and SPECT for the diagnosis of coronary artery disease: a head-to-head comparison from the CORE320 multicenter diagnostic performance study. *Radiology* 274(2):626
- Goetti R, Reiner CS, Knuth A, Klotz E, Stenner F, Samaras P, Alkadhi H (2012) Quantitative perfusion analysis of malignant liver tumors: dynamic computed tomography and contrast-enhanced ultrasound. *Invest Radiol* 47(1):18–24
- Gordic S, Husarik DB, Desbiolles L, Leschka S, Frauenfelder T, Alkadhi H (2014a) High-pitch coronary CT angiography with third generation dual-source CT: limits of heart rate. *Int J Cardiovasc Imaging* 30(6):1173–1179
- Gordic S, Morsbach F, Schmidt B et al (2014b) Ultralow-dose chest computed tomography for pulmonary nodule detection: first performance evaluation of single energy scanning with spectral shaping. *Invest Radiol* 49(7):465–473
- Grant KL, Flohr TG, Krauss B et al (2014) Assessment of an advanced image-based technique to calculate virtual monoenergetic CT images from a dual-energy examination to improve contrast-to-noise ratio in examinations using iodinated contrast media. *Invest Radiol* 49(9):586–592

- Grass M, Köhler T, Proksa R (2000) 3D cone-beam CT reconstruction for circular trajectories. *Phys Med Biol* 45(2):329–347
- Hague CJ, Krowchuk N, Alhassan D, Ho K, Leipsic J, Sin DD, Mayo JR, Coxson HO (2014) Qualitative and quantitative assessment of smoking-related lung disease: effect of iterative reconstruction on low-dose computed tomographic examinations. *J Thorac Imaging* 29(6):350–356
- Hein I, Taguchi K, Silver MD, Kazarna M, Mori I (2003) Feldkamp-based cone-beam reconstruction for gantry-tilted helical multislice CT. *Med Phys* 30(12):3233–3242
- Henzler T, Fink C, Schoenberg SO, Dual SUJ, Energy CT (2012) Radiation dose aspects. *AJR* 199:S16–S25
- Hou DJ, Tso DK, Davison C, Inacio J, Louis LJ, Nicolaou S, Reimann AJ, Hou DJ, Tso DK, Davison C, Inacio J, Louis LJ, Nicolaou S, Reimann AJ (2013) Clinical utility of ultra high pitch dual source thoracic CT imaging of acute pulmonary embolism in the emergency department: are we one step closer towards a non-gated triple rule out? *Eur J Radiol* 82(10):1793–1798
- Hutt A, Tacelli N, Faivre JB, Flohr T, Duhamel A, Remy J, Remy-Jardin M (2016) Is bronchial wall imaging affected by temporal resolution? comparative evaluation at 140 and 75 ms in 90 patients. *Eur Radiol* 26(2):469–477
- Johnson TR, Nikolaou K, Wintersperger BJ, Knez A, Boekstegers P, Reiser MF, Becker CR (2007a) ECG-gated 64-MDCT angiography in the differential diagnosis of acute chest pain. *Am J Roentgenol* 188(1):76–82
- Johnson TR, Nikolaou K, Busch S, Leber AW, Becker A, Wintersperger BJ, Rist C, Knez A, Reiser MF, Becker CR (2007b) Diagnostic accuracy of dual-source computed tomography in the diagnosis of coronary artery disease. *Invest Radiol* 42(10):684–691
- Kang EJ, Lee KN, Kim DW, Kim BS, Choi S, Park BH, Oh JY (2012) Triple rule-out acute chest pain evaluation using a 320-row-detector volume CT: a comparison of the wide-volume and helical modes. *Int J Cardiovasc Imaging* 28(Suppl 1):7–13
- Kim Y, Kim YK, Lee BE, Lee SJ, Ryu YJ, Lee JH, Chang JH (2015) Ultra-low-dose CT of the thorax using iterative reconstruction: evaluation of image quality and radiation dose reduction. *AJR Am J Roentgenol* 204(6):1197–1202
- Knez A, Becker CR, Leber A, Ohnesorge B, Becker A, White C, Haberl R, Reiser MF, Steinbeck G (2001) Usefulness of multislice spiral computed tomography angiography for determination of coronary artery stenoses. *Am J Clin Pathol* 88:1191–1194
- Kondo T, Kumamaru KK, Fujimoto S, Matsutani H, Sano T, Takase S, Rybicki FJ (2013) Prospective ECG-gated coronary 320-MDCT angiography with absolute acquisition delay strategy for patients with persistent atrial fibrillation. *AJR Am J Roentgenol* 201(6):1197–1203
- Leber AW, Knez A, von Ziegler F, Becker A, Nikolaou K, Paul S, Wintersperger B, Reiser M, Becker CR, Steinbeck G, Boekstegers P (2005) Quantification of obstructive and nonobstructive coronary lesions by 64-slice computed tomography. *JACC* 46(1):147–154
- Lee AM, Engel LC, Shah B, Liew G, Sidhu MS, Kalra M, Abbara S, Brady TJ, Hoffmann U, Ghoshhajra BB (2012) Coronary computed tomography angiography during arrhythmia: radiation dose reduction with prospectively ECG-triggered axial and retrospectively ECG-gated helical 128-slice dual-source CT. *J Cardiovasc Comput Tomogr* 6(3):172–183.e2
- Leipsic J, Nguyen G, Brown J, Sin D, Mayo JR (2010) A prospective evaluation of dose reduction and image quality in chest CT using adaptive statistical iterative reconstruction. *AJR Am J Roentgenol* 195(5):1095–1099
- Lell M, Hinkmann F, Anders K, Deak P, Kalender WA, Uder M, Achenbach S (2009) High-pitch electrocardiogram-triggered computed tomography of the chest: initial results. *Invest Radiol* 44(11):728–733
- Lell MM, May M, Deak P, Alibek S, Kuefner M, Kuettner A, Köhler H, Achenbach S, Uder M, Radkowi T (2011) High-pitch spiral computed tomography: effect on image quality and radiation dose in pediatric chest computed tomography. *Invest Radiol* 46(2):116–123
- Leschka S, Stolzmann P, Desbiolles L, Baumüller S, Goetti R, Schertler T, Scheffel H, Plass A, Falk V, Feuchtnner G, Marincek B, Alkadhi H (2009) Diagnostic accuracy of high-pitch dual-source CT for the assessment of coronary stenoses: first experience. *Eur Radiol* 19(12):2896–2903
- Lu GM, Zhao Y, Zhang LJ, Schoepf UJ (2012) Dual-energy CT of the lung. *AJR Am J Roentgenol* 199(5 Suppl):S40–S53
- Manniesing R, Oei MT, van Ginneken B, Prokop M (2016) Quantitative dose dependency analysis of whole-brain CT perfusion imaging. *Radiology* 278(1):190–197
- McCollough CH, Primak AN, Braun N, Kofler J, Yu L, Christner J (2009) Strategies for reducing radiation dose in CT. *Radiol Clin North Am* 47(1):27–40
- Meier A, Wurnig M, Desbiolles L, Leschka S, Frauenfelder T, Alkadhi H (2015) Advanced virtual monoenergetic images: improving the contrast of dual-energy CT pulmonary angiography. *Clin Radiol* 70(11):1244–1251
- Meinel FG, Canstein C, Schoepf UJ, Sedlmaier M, Schmidt B, Harris BS, Flohr TG, De Cecco CN (2014) Image quality and radiation dose of low tube voltage 3rd generation dual-source coronary CT angiography in obese patients: a phantom study. *Eur Radiol* 24(7):1643–1650
- Mets OM, Willeminck MJ, de Kort FP, Mol CP, Leiner T, Oudkerk M, Prokop M, de Jong PA (2012) The effect of iterative reconstruction on computed tomography assessment of emphysema, air trapping and airway dimensions. *Eur Radiol* 22(10):2103–2109
- Meyer M, Haubenreisser H, Schoepf UJ, Vliegenthart R, Leidecker C, Allmendinger T, Lehmann R, Sudarski S, Borggrefe M, Schoenberg SO, Henzler T (2014) Closing in on the K edge: coronary CT angiography at 100, 80, and 70 kV-initial comparison of a second-

- versus a third-generation dual-source CT system. *Radiology* 273(2):373–382
- Morhard D, Wirth CD, Fesl G, Schmidt C, Reiser MF, Becker CR, Ertl-Wagner B (2010) Advantages of extended brain perfusion computed tomography: 9.6 cm coverage with time resolved computed tomography-angiography in comparison to standard stroke-computed tomography. *Invest Radiol* 45(7):363–369
- Morsbach F, Gordic S, Desbiolles L, Husarik D, Frauenfelder T, Schmidt B, Allmendinger T, Wildermuth S, Alkadhi H, Leschka S (2014) Performance of turbo high-pitch dual-source CT for coronary CT angiography: first ex vivo and patient experience. *Eur Radiol* 24(8):1889–1895
- Motosugi U, Ichikawa T, Sou H, Morisaka H, Sano K, Araki T (2012) Multi-organ perfusion CT in the abdomen using a 320-detector row CT scanner: preliminary results of perfusion changes in the liver, spleen, and pancreas of cirrhotic patients. *Eur J Radiol* 81(10):2533–2537
- Newell JD Jr, Fuld MK, Allmendinger T, Sieren JP, Chan KS, Guo J, Hoffman EA (2015) Very low-dose (0.15 mGy) chest CT protocols using the COPDGene 2 test object and a third-generation dual-source CT scanner with corresponding third-generation iterative reconstruction software. *Invest Radiol* 50(1):40–45
- Nieman K, Oudkerk M, Rensing BJ, van Ooijen P, Munne A, van Geuns RJ, de Feyter PJ (2001) Coronary angiography with multi-slice computed tomography. *Lancet* 357:599–603
- Niemann T, Henry S, Faivre JB, Yasunaga K, Bendaoud S, Simeone A, Remy J, Duhamel A (2013) Clinical evaluation of automatic tube voltage selection in chest CT angiography. *Eur Radiol* 23(10):2643–2651
- Niemann T, Henry S, Duhamel A, Faivre JB, Deschildre A, Colas L, Santangelo T, Remy J, Remy-Jardin M (2014) Pediatric chest CT at 70 kVp: a feasibility study in 129 children. *Pediatr Radiol* 44(11):1347–1357
- Ohnesorge B, Flohr T, Becker C, Kopp A, Schoepf U, Baum U, Knez A, Klingenbeck Regn K, Reiser M (2000) Cardiac imaging by means of electro-cardiographically gated multisection spiral CT – initial experience. *Radiology* 217:564–571
- Ohno Y, Koyama H, Matsumoto K, Onishi Y, Takenaka D, Fujisawa Y, Yoshikawa T, Konishi M, Maniwa Y, Nishimura Y, Ito T, Sugimura K (2011) Differentiation of malignant and benign pulmonary nodules with quantitative first-pass 320-detector row perfusion CT versus FDG PET/CT. *Radiology* 258(2):599–609
- Padole A, Singh S, Ackman JB, Wu C, Do S, Pourjabbar S, Khawaja RD, Otrakji A, Digumarthy S, Shepard JA, Kalra M (2014) Submillisievert chest CT with filtered back projection and iterative reconstruction techniques. *AJR Am J Roentgenol* 203(4):772–781
- Pansini V, Remy-Jardin M, Faivre JB et al (2009) Assessment of lobar perfusion in smokers according to the presence and severity of emphysema: preliminary experience with dual-energy CT angiography. *Eur Radiol* 19(12):2834–2843
- Paul JF, Amato A, Rohnean A (2013) Low-dose coronary-CT angiography using step and shoot at any heart rate: comparison of image quality at systole for high heart rate and diastole for low heart rate with a 128-slice dual-source machine. *Int J Cardiovasc Imaging* 29(3):651–657
- Petersilka M, Bruder H, Krauss B, Stierstorfer K, Flohr TG (2008) Technical principles of dual source CT. *Eur J Radiol* 68(3):362–368
- Petersilka M, Stierstorfer K, Bruder H, Flohr T (2010) Strategies for scatter correction in dual source CT. *Med Phys* 37(11):5971–5992
- Plank F, Friedrich G, Bartel T, Mueller S, Bonaros N, Heinz A, Klauser A, Cartes-Zumelzu F, Grimm M, Feuchtner G (2012) Benefits of high-pitch 128-slice dual-source computed tomography for planning of transcatheter aortic valve implantation. *Ann Thorac Surg* 94(6):1961–1966
- Pontana F, Faivre JB, Remy-Jardin M, Flohr T, Schmidt B, Tacelli N, Pansini V, Remy J (2008) Lung perfusion with dual-energy multidetector-row CT (MDCT): feasibility for the evaluation of acute pulmonary embolism in 117 consecutive patients. *Acad Radiol* 15(12):1494–1504
- Pontana F, Pagniez J, Flohr T, Faivre JB, Duhamel A, Remy J, Remy-Jardin M (2011a) Chest computed tomography using iterative reconstruction vs filtered back projection (part 1): evaluation of image noise reduction in 32 patients. *Eur Radiol* 21(3):627–635
- Pontana F, Duhamel A, Pagniez J, Flohr T, Faivre JB, Hachulla AL, Remy J, Remy-Jardin M (2011b) Chest computed tomography using iterative reconstruction vs filtered back projection (part 2): image quality of low-dose CT examinations in 80 patients. *Eur Radiol* 21(3):636–643
- Pontana F, Henry S, Duhamel A, Faivre JB, Tacelli N, Pagniez J, Remy J, Remy-Jardin M (2015) Impact of iterative reconstruction on the diagnosis of acute pulmonary embolism (PE) on reduced-dose chest CT angiograms. *Eur Radiol* 25(4):1182–1189
- Prakash P, Kalra MK, Digumarthy SR, Hsieh J, Pien H, Singh S, Gilman MD, Shepard JA (2010) Radiation dose reduction with chest computed tomography using adaptive statistical iterative reconstruction technique: initial experience. *J Comput Assist Tomogr* 34(1):40–45
- Raff GL, Gallagher MJ, O'Neill WW, Goldstein JA (2005) Diagnostic accuracy of noninvasive coronary angiography using 64-slice spiral computed tomography. *JACC* 46(3):552–557
- Remy-Jardin M, Remy J (2008) Vascular disease in chronic obstructive pulmonary disease. *Proc Am Thorac Soc* 5(9):891–899
- Remy-Jardin J, Tillie-Leblond I, Szapiro D et al (2002) CT angiography of pulmonary embolism in patients with underlying respiratory disease: impact of multislice CT on image quality and negative predictive value. *Eur Radiol* 12:1971–1978
- Remy-Jardin M, Faivre JB, Pontana F, Molinari F, Tacelli N, Remy J (2014) Thoracic applications of dual energy. *Semin Respir Crit Care Med* 35(1):64–73

- Rybicki FJ, Otero HJ, Steigner ML, Vorobiof G, Nallamshetty L, Mitsouras D, Ersoy H, Mather RT, Judy PF, Cai T, Coyner K, Schultz K, Whitmore AG, Di Carli MF (2008) Initial evaluation of coronary images from 320-detector row computed tomography. *Int J Cardiovasc Imaging* 24(5):535–546
- Salem R, Remy-Jardin M, Delhaye D, Khalil C, Teisseire A, Delannoy-Deken V, Duhamel A, Remy J (2006) Integrated cardio-thoracic imaging with ECG-Gated 64-slice multidetector-row CT: initial findings in 133 patients. *Eur Radiol* 16(9):1973–1981
- Schenzle JC, Sommer WH, Neumaier K et al (2010) Dual energy CT of the chest: how about the dose? *Invest Radiol* 45:347–353
- Schoepf UJ (2007) Cardiothoracic multi-slice CT in the Emergency Department. In: Ohnesorge BM, Flohr TG, Becker CR, Knez A, Reiser MF (eds) *Multi-slice and dual-source CT in cardiac imaging*, 2nd edn. Springer, Berlin/Heidelberg/New York
- Schoepf UJ, Kessler MA, Rieger CT et al (2001) Multislice CT imaging of pulmonary embolism. *Eur Radiol* 11:2278–2286
- Schoepf UJ, Holzknacht N, Helmberger TK et al (2002) Subsegmental pulmonary emboli: improved detection with thin-collimation multidetector row spiral CT. *Radiology* 222:483–490
- Schoepf UJ, Becker CR, Hofmann LK, Das M, Flohr T, Ohnesorge BM et al (2003) Multislice CT angiography. *Eur Radiol* 13:1946–1961
- Schulz B, Jacobi V, Beeres M, Bodelle B, Gruber T, Lee C, Bauer R, Kerl M, Vogl T, Zangos S (2012) Quantitative analysis of motion artifacts in high-pitch dual-source computed tomography of the thorax. *J Thorac Imaging* 27(6):382–386
- Sharma RK, Arbab-Zadeh A, Kishi S, Chen MY, Magalhães TA, George RT, Dewey M, Rybicki FJ, Kofoed KF, de Roos A, Tan SY, Matheson M, Vavere A, Cox C, Clouse ME, Miller JM, Brinker JA, Arai AE, Di Carli MF, Rochitte CE, Lima JA (2015) Incremental diagnostic accuracy of computed tomography myocardial perfusion imaging over coronary angiography stratified by pre-test probability of coronary artery disease and severity of coronary artery calcification: The CORE320 study. *Int J Cardiol* 201:570–577
- Singh S, Kalra MK, Gilman MD, Hsieh J, Pien HH, Digumarthy SR, Shepard JA (2011) Adaptive statistical iterative reconstruction technique for radiation dose reduction in chest CT: a pilot study. *Radiology* 259(2):565–573
- Sommer WH, Helck A, Bamberg F, Albrecht E, Becker CR, Weidenhagen R, Kramer H, Reiser MF, Nikolaou K (2010) Diagnostic value of time-resolved CT angiography for the lower leg. *Eur Radiol* 20(12):2876–2881
- Sommer WH, Becker CR, Haack M, Rubin GD, Weidenhagen R, Schwarz F, Nikolaou K, Reiser MF, Johnson TR, Clevert DA (2012) Time-resolved CT angiography for the detection and classification of endoleaks. *Radiology* 263(3):917–926
- Steigner ML, Otero HJ, Cai T, Mitsouras D, Nallamshetty L, Whitmore AG, Ersoy H, Levit NA, Di Carli MF, Rybicki FJ (2009) Narrowing the phase window width in prospectively ECG-gated single heart beat 320-detector row coronary CT angiography. *Int J Cardiovasc Imaging* 25(1):85–90
- Stierstorfer K, Rauscher A, Boese J, Bruder H, Schaller S, Flohr T (2004) Weighted FBP—a simple approximate 3D FBP algorithm for multislice spiral CT with good dose usage for arbitrary pitch. *Phys Med Biol* 49:2209–2218
- Sun ML, Lu B, Wu RZ, Johnson L, Han L, Liu G, Yu FF, Hou ZH, Gao Y, Wang HY, Jiang S, Yang YJ, Qiao SB (2011) Diagnostic accuracy of dual-source CT coronary angiography with prospective ECG-triggering on different heart rate patients. *Eur Radiol* 21(8):1635–1642
- Tacelli N, Remy-Jardin M, Flohr T, Faivre JB, Delannoy V, Duhamel A, Remy J (2010) Dual-source chest CT angiography with high temporal resolution and high pitch modes: evaluation of image quality in 140 patients. *Eur Radiol* 20(5):1188–1196
- Thibault JB, Sauer KD, Bouman CA, Hsieh J (2007) A three-dimensional statistical approach to improved image quality for multislice helical CT. *Med Phys* 34(11):4526–4544
- Thieme SF, Becker CR, Hacker M, Nikolaou K, Reiser MF, Johnson TR (2008) Dual energy CT for the assessment of lung perfusion—correlation to scintigraphy. *Eur J Radiol* 68(3):369–374
- Thieme SF, Johnson TR, Lee C, McWilliams J, Becker CR, Reiser MF, Nikolaou K (2009) Dual-energy CT for the assessment of contrast material distribution in the pulmonary parenchyma. *AJR Am J Roentgenol* 193(1):144–149
- Tkaczyk JE, Rodrigues R, Shaw J, Short J, Du Y, Wu X, Walter D, Leue W, Harrison D, Edic P (2007) Atomic number resolution for three spectral CT imaging systems. *Proc of SPIE Vol 6510*:651009
- Tomizawa N, Maeda E, Akahane M, Torigoe R, Kiryu S, Ohtomo K (2013) Coronary CT angiography using the second-generation 320-detector row CT: assessment of image quality and radiation dose in various heart rates compared with the first-generation scanner. *Int J Cardiovasc Imaging* 29(7):1613–1618
- Vardhanabhuti V, Loader RJ, Mitchell GR, Riordan RD, Roobottom CA (2013) Image quality assessment of standard- and low-dose chest CT using filtered back projection, adaptive statistical iterative reconstruction, and novel model-based iterative reconstruction algorithms. *AJR Am J Roentgenol* 200(3):545–552
- Wang G, Zhang C, Li M, Deng K, Li W (2014) Preliminary application of high-definition computed tomographic Gemstone Spectral Imaging in lung cancer. *J Comput Assist Tomogr* 38(1):77–81
- Wang R, Sui X, Schoepf UJ, Song W, Xue H, Jin Z, Schmidt B, Flohr TG, Canstein C, Spearman JV, Chen J, Meinel FG (2015) Ultralow-radiation-dose chest CT: accuracy for lung densitometry and emphysema detection. *AJR Am J Roentgenol* 204(4):743–749

- Westwood ME, Raatz HD, Misso K, Burgers L, Redekop K, Lhachimi SK, Armstrong N, Kleijnen J (2013) Systematic review of the accuracy of dual-source cardiac CT for detection of arterial stenosis in difficult to image patient groups. *Radiology* 267(2):387–395
- Willems PW, Taashineetanakul P, Schenk B, Brouwer PA, Terbrugge KG, Krings T (2012) The use of 4D-CTA in the diagnostic work-up of brain arteriovenous malformations. *Neuroradiology* 54(2):123–131
- Wuest W, Anders K, Schuhbaeck A, May MS, Gauss S, Marwan M, Arnold M, Ensminger S, Muschiol G, Daniel WG, Uder M, Achenbach S (2012) Dual source multidetector CT-angiography before Transcatheter Aortic Valve Implantation (TAVI) using a high-pitch spiral acquisition mode. *Eur Radiol* 22(1):51–58
- Zhang D, Li X, Liu B (2011) Objective characterization of GE discovery CT750 HD scanner: gemstone spectral imaging mode. *Med Phys* 38(3):1178–1188